Accepted Manuscript

Senescent hepatocytes in decompensated liver show reduced UPR^{MT} and its key player, CLPP, attenuates senescence *in vitro*

Bijoya Sen, Archana Rastogi, Rhisita Nath, Saggere M. Shasthry, Viniyendra Pamecha, Sonika Pandey, Kapuganti J. Gupta, Shiv K. Sarin, Nirupma Trehanpati, Gayatri Ramakrishna

PII: S2352-345X(19)30027-X
DOI: https://doi.org/10.1016/j.jcmgh.2019.03.001
Reference: JCMGH 459

To appear in: *Cellular and Molecular Gastroenterology and Hepatology*
Accepted Date: 1 March 2019

Please cite this article as: Sen B, Rastogi A, Nath R, Shasthry SM, Pamecha V, Pandey S, Gupta KJ, Sarin SK, Trehanpati N, Ramakrishna G, Senescent hepatocytes in decompensated liver show reduced UPR^{MT} and its key player, CLPP, attenuates senescence *in vitro*, *Cellular and Molecular Gastroenterology and Hepatology* (2019), doi: https://doi.org/10.1016/j.jcmgh.2019.03.001.

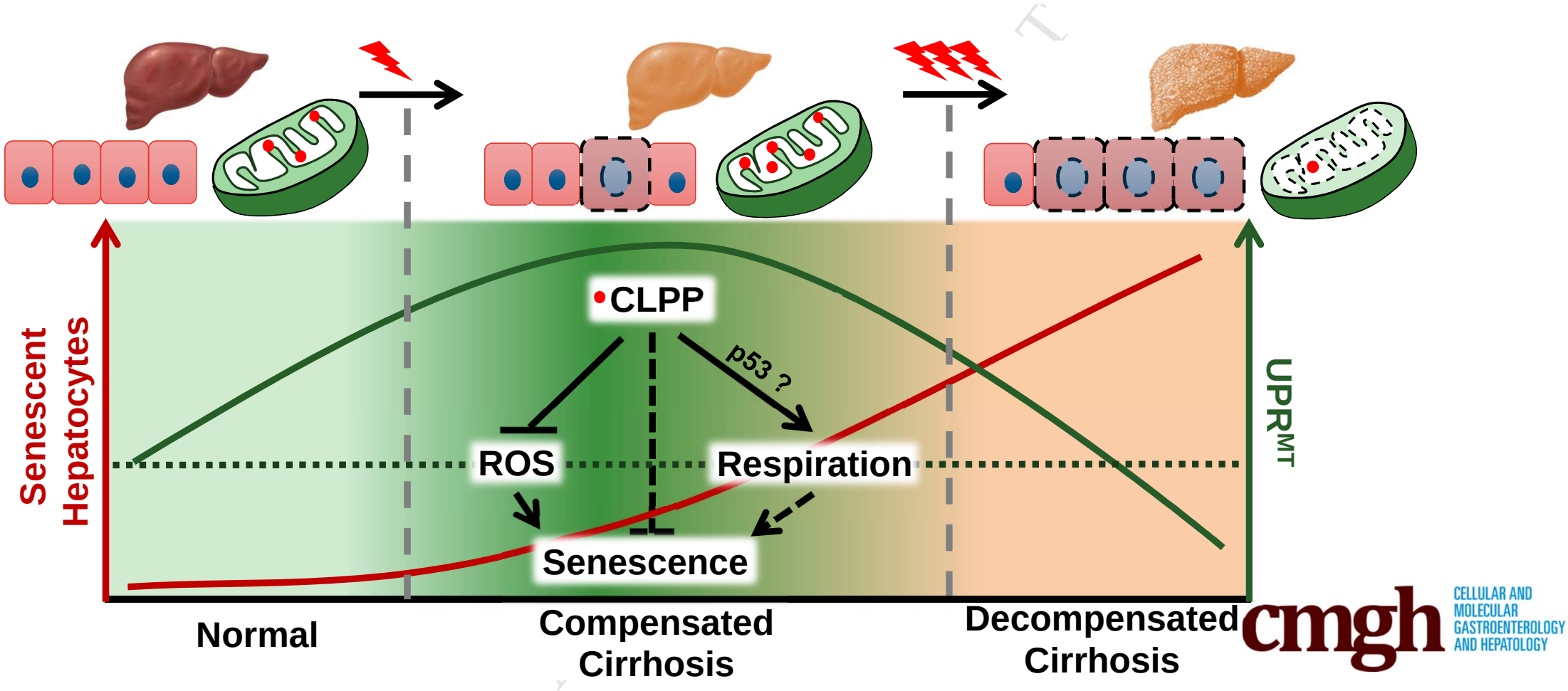

cmgh CELLULAR AND MOLECULAR GASTROENTEROLOGY AND HEPATOLOGY

Senescent hepatocytes in decompensated liver show reduced UPR^{MT} and its key player, CLPP, attenuates senescence *in vitro*

Bijoya Sen[1], Archana Rastogi[2], Rhisita Nath[1], Saggere M. Shasthry[3], Viniyendra Pamecha[4], Sonika Pandey[5], Kapuganti J. Gupta[5], Shiv K. Sarin[3], Nirupma Trehanpati[1] and Gayatri Ramakrishna[1#]

Affiliations

1. Molecular and Cellular Medicine, Institute of Liver and Biliary Sciences, New Delhi, India
2. Pathology, Institute of Liver and Biliary Sciences, New Delhi, India
3. Hepatology, Institute of Liver and Biliary Sciences, New Delhi, India
4. Hepato Pancreato Biliary and Liver Transplant Surgery, Institute of Liver and Biliary Sciences, New Delhi, India
5. National Institute of Plant Genome Research, New Delhi, India

 # Corresponding Author and address:

Gayatri Ramakrishna, PhD
Dept of Molecular and Cellular Medicine
Institute of Liver and Biliary Sciences (ILBS)
D1 Block, Vasant Kunj,
Delhi-110070,
India
Phone: +91-11-46300000, Ext 24143
FAX: +91-11-26123504
Email: rgayatri@ilbs.in, gayatrirama1@gmail.com

Running title: CLPP attenuates hepatocyte senescence

Word count: 4361 (excluding methods, tables, figure legends and references)

Conflict of interest: The authors declare that they have no conflict of interest.

Authors Contribution: BS: Performed all experiments, compiled and analysed data, and inputs in manuscript writing, GR: Conceived and designed study, analysed data and wrote manuscript, RN: helped in experimental protocols; AR: Read pathology slides and gave clinical inputs, NT: Helped in FACS and provided research inputs; VP and SMS: provided clinical samples, diagnosis, SKS: Clinical inputs and manuscript editing, KJG and SP: helped in mitochondrial respiration assay using Clarke's electrode.

Synopsis:

Compensated cirrhosis exhibited a marked increase in mitochondrial unfolded protein response with the high levels of CLPP. However, decompensated cirrhosis showed reduced UPR^{MT} with a significant increase in number of senescent hepatocytes. Over-expression of CLPP in an *in vitro* model of premature senescence could significantly reduce senescence associated phenotype by inhibiting mitochondrial ROS and altering mitochondrial respiration.

Abstract:

Background and Aims: Non-dividing hepatocytes in end-stage liver disease indicates permanent growth arrest similar to senescence. Identifying senescence *in vivo* is often challenging and mechanisms inhibiting senescence are poorly understood. In lower organisms mitochondrial unfolded protein response (UPR^{MT}) helps in increasing longevity; however, its role in senescence and liver disease is poorly understood. Aim of this study was to identify hepatocyte senescence and role of UPR^{MT} in cryptogenic cirrhosis.

Methods: Doxorubicin was used to induce senescence in non-neoplastic hepatocytes (PH5CH8) and hepatoma cells (HepG2 and Huh7). Senescence-associated markers and unfolded protein response was evaluated by fluorescence microscopy, immunoblotting and gene expression. Explants/biopsies from normal, fibrosis, compensated and decompensated cirrhosis without any known etiology were examined for presence of senescence and UPR^{MT} by immunohistochemistry and gene expression.

Results: Accumulation of senescent hepatocytes in cryptogenic cirrhosis was associated with reduced proliferation, increased expression of γH2AX and p21, together with loss of LaminB1. Dysfunctional mitochondria and compromised UPR^{MT} were key features of senescent hepatocytes both *in vitro* and also in decompensated cirrhosis. Intriguingly, compensated cirrhotic liver mounted strong UPR^{MT}, with high levels of mitochondrial protease, CLPP. Over-expression of CLPP inhibited senescence *in vitro*, by reducing mitochondrial ROS and altering oxygen consumption.

Conclusions: Our results implicate a role of hepatocyte senescence in cryptogenic cirrhosis together with a crucial role of UPR^{MT} in preventing hepatocyte senescence. A compromised UPR^{MT} may shift the fate of cirrhotic liver towards decompensation by exaggerating hepatocyte senescence. Restoring CLPP levels at least in cell culture appears as a promising strategy in mitohormesis, thereby, preventing senescence and possibly improving hepatocyte function.

Keywords: Cryptogenic liver cirrhosis, Mitochondrial respiration, Mitochondrial unfolded protein response, Oxidative stress

Introduction

Liver injury usually leads to high turnover of cells which includes both cellular death and regeneration. During chronic liver injury, impairment in regenerative capacity results in functional insufficiency, often culminating in cirrhosis which is also clinically regarded as end-stage liver disease. Two distinct sub-clinical stages have been proposed for cirrhosis which includes (a) an early compensated phase with or without varices and (b) a late decompensated phase with life threatening complications such as variceal haemorrhage, ascites, UGI bleed or hepatic encephalopathy [1]. The evolution of cirrhosis involves a pathological transition from highly regenerating nodules in compensated state to explicatively exhausted hepatocytes during decompensated state, finally culminating in parenchymal extinction [1]. There are a few questions still unanswered regarding the cirrhotic evolution: what tips the balance in favour of a decompensated state and what mechanisms rescues hepatocytes from growth inhibition. In chronic liver disease, hepatocyte damage leading to cell death has been extensively studied, while the process of cellular senescence which prevents hepatocyte proliferation is relatively less explored. A senescent hepatocyte is permanently growth arrested which inhibits liver regeneration and contributes to disease progression. Evidence now strongly point towards existence of senescent hepatocytes in various liver diseases related to alcohol, HCV and fatty liver [2-4]. Mechanisms involved in hepatocyte senescence are poorly understood. Some studies have highlighted the role of cell cycle inhibitors like p21, TGFβ and telomere shortening in hepatocyte growth arrest and senescence [2, 5-7]. Cellular senescence due to telomere attrition is usually a slow process; however oxidative damage usually results in accelerated ageing and often referred as stress induced premature senescence (SIPS). Oxidative damage is often a hallmark feature in cirrhotic liver [8, 9], which in turn implicates its role in genesis of senescent hepatocytes.

Mitochondria are the main sources of reactive oxygen species and considered a main cause of ageing [10]. Hepatocytes are rich in mitochondria and altered mitochondrial functions have been documented in a variety of chronic liver diseases [11]. Maintaining the mitochondrial function and removal of defective mitochondria are therefore important in preventing senescent changes and in maintenance of organ homeostasis. Dysfunctional mitochondria are removed by the process of mitophagy which is often defective in senescence [12]. Defective mitophagy has been well studied in the context of liver disease [13, 14]. Recent studies have pointed to the existence of yet another cellular mechanism, named mitochondrial unfolded protein response (UPR^{MT}) involving mitochondrial-to-nuclear communication/retrograde response for recovery of dysfunctional mitochondria [15]. This protein quality control mechanism is well studied in model organisms, such as yeast, *C. elegans*, *D. melanogaster* etc. Work in *C. elegans* has revealed a link between UPR^{MT} and enhanced longevity [16]. This in turn implicates a role of UPR^{MT} during aging including senescence. However, the role of UPR^{MT} in the context of mammalian senescence is not well studied. As senescence is a stress

response, it is essential to evaluate the role of UPR^{MT} in this process. Senescent cells often accumulate in disease conditions, such as cirrhosis; there are hardly any data available on relevance of UPR^{MT} in End Stage Liver disease (ESLD). Recently, two papers have highlighted contradictory roles of UPR^{MT} in liver. Gariani *et al*. reported that NAD^+ replenishment promoted UPR^{MT} to prevent fatty liver [17]. On the other hand deletion of mitochondrial protease, CLPP, a key player of UPR^{MT}, protected mice from development of fatty liver when fed a high fat diet [18, 19].

Identifying senescence in clinical specimens is often challenging and mechanisms involved in hepatocyte senescence are poorly understood. Further, strategies averting hepatocyte growth inhibition due to senescence appears crucial in preventing liver disease. As mitochondrial dysfunctions accompany liver disease, we hypothesized that alterations in mitochondrial stress response pathway viz., UPR^{MT}, may accompany senescent associated changes during progression of liver disease and key players of UPR^{MT} can ameliorate hepatocyte senescence. Aim of the present study was to identify senescence-associated markers together with alterations in UPR^{MT} pathway using, first an *in vitro* model of doxorubicin induced hepatocyte senescence and secondly during progression of end stage liver disease in cryptogenic liver disease. There is hardly any information available on the molecular events associated with development of cryptogenic liver disease. Also, other forms of basic insults, such as alcohol, viruses or fatty liver disease etc might involve mitochondrial damage as part of pathogenesis of cirrhosis. Hence, the choice of cryptogenic cirrhosis as it would provide better insights into the role of UPR^{MT} exclusive to cirrhosis and not confounded by other risk factors. Accordingly, we hypothesized a role of deregulated UPR^{MT} and hepatocyte senescence in synergistically contributing towards the pathogenesis of cryptogenic liver disease.

Briefly, the work revealed accumulation of senescent hepatocytes in decompensated cirrhosis and compromised UPR^{MT} as a key senescence-associated feature. Intriguingly, a strong UPR^{MT} in compensated cirrhosis indicated its possible role in survival. This work also highlights the role of mitochondrial protease, CLPP, which is a key player of UPR^{MT} in preventing stress induced premature senescence at least in cell culture system.

RESULTS

Low dose of Doxorubicin induces permanent growth arrest similar to senescence in hepatoma cells.

In a previous work we had demonstrated that low dose of doxorubicin induced senescence in osteosarcoma cells [20]. To test if hepatoma cells (HepG2 and Huh7) can also show senescence like changes, cells were treated with doxorubicin for 2hr with different doses ranging from 0.5-5µM, followed by change into fresh medium and growth was monitored for 6 days. A 2µM dose of doxorubicin showed maximum growth arrest by 6^{th} day in both the cell lines (Fig. 1A). Flow

cytometry analysis showed that doxorubicin treatment resulted in significant growth arrest as revealed by two to three fold increase in percentage of cells in the G2/M phase of cell cycle in hepatoma cells. In comparison to G2M arrest, the percentage cell death as indicated by sub G0 cells was considerably less in doxorubicin treated cells (Fig. 1B). To test if the doxorubicin treated cells were permanently growth arrested, cells were stimulated with 10% serum and immunocytochemsitry was performed for proliferation marker, Ki67. Compared to control, the doxorubicin treated cells on 6^{th} day showed fewer number of Ki67 positive nuclei indicating growth arrest (Fig. 1C, D). HepG2 cells with wild type p53, showed more prominent growth arrest compared to Huh7 harbouring mutant p53.

Doxorubicin treated HepG2 and Huh7 cells under bright field microscope showed enlarged and flattened morphology and a significant increase in Senescence Associated-β-galactosidase (SA-β-gal) positivity (>90%) on the 6^{th} day of treatment indicative of premature senescence (Fig. 2A). Other senescence-associated markers were evaluated by both immunoblot assay and confocal microscopy. Premature senescence in doxorubicin treated cells was associated with increase in levels of DNA damage marker, γH2AX and also a heterochromatin associated repressive marker, $H_3K_9me_3$ (Fig. 2B, C, D). The inhibitor of cyclin dependent kinases, p21 which results in growth arrest was prominently increased in the doxorubicin treated HepG2 cells. As p21 is a transcriptional target of p53, its levels were hardly detected in Huh7 cells harboring dysfunctional p53 (Fig. 2B). The changes in above markers were also associated with a prominent loss in nuclear lamina protein, LaminB1, which was confirmed by immunoblotting as well as imaging (Fig. 2B, C, D). Doxorubicin treated HepG2 and Huh7 cells also showed a distinct senescence associated secretory phenotype (SASP) which is described in detail in later section (see Fig. 9D). These results indicated that treatment with low dose of doxorubicin induced senescent features in hepatoma cells regardless of their p53 status. Hence, hereafter the doxorubicin treated cells are referred as senescent cells.

Doxorubicin induced premature senescence is associated with mitochondrial dysfunction and compromised UPR^{MT}

Transmission electron microscopy (TEM) revealed fewer and enlarged mitochondria in senescent HepG2 and Huh7 cells (Fig. 3A). Unlike the control cells which showed well placed stacks of mitochondrial cristae, the senescent cells showed incomplete and disrupted cristae. Mitochondrial membrane potential (MMP) was measured using a mitochondrial membrane potential sensitive dye, TMRE. Senescent HepG2 cells showed more accumulation of TMRE than control cells suggestive of hyperpolarized mitochondria (Fig. 3B). In contrast, the Huh7 cells showed fourfold decrease in TMRE accumulation, indicating mitochondrial depolarization. The TMRE results were also corroborated by yet another MMP sensitive agent, Mitotracker red, which showed enhanced intensity in senescent HepG2 cells but feeble in senescent Huh7 cells (Fig. 3C).

As oxidative stress is an underlying cause of cellular senescence we stained the cells with MitoSOX, a specific indicator of mitochondrial superoxide. Senescent HepG2 and Huh7 cells showed increase in levels of MitoSOX, as analysed by flow cytometry (Fig. 3D). Next, we evaluated if mitochondrial dysfunction is related to mitochondrial content. For this the mtDNA content relative to nuclear DNA content (mtDNA/nDNA) was measured by real-time qPCR. The senescent cells showed a significant decrease in mtDNA (Fig. 3E). Since mitochondrial biogenesis is also responsible for the mitochondrial mass, we evaluated the expression levels of various genes involved in its biogenesis. PGC1α showed increased expression following senescence, while its downstream targets such as TFAM, NRF1 and NRF2α showed downregulation (Fig. 3F).

In a model organism, *C. elegans*, it has been shown that defects in mitochondria lead to activation of a stress response pathway viz., the UPR^{MT}. Some key players of UPR^{MT} pathway were therefore analyzed in senescent cells by both real time PCR and immunoblotting. Senescent HepG2 and Huh7 cells showed a significant decline in transcript levels of mitochondrial matrix proteases CLPP and YME1L1; mitochondrial chaperone, HSP60 and a transcription factor ATF5, (Fig. 4A). Further immunoblotting revealed two fold reductions in key players of UPR^{MT} pathway viz., HSP60, HSP10 and CLPP (Fig. 4B), thereby indicating compromised UPR^{MT} response during senescence.

Cryptogenic cirrhotic liver showed accumulation of senescent hepatocytes and an altered UPR^{MT}

Having identified the senescence-associated markers in the *in vitro* study, we evaluated if the above markers can also identify senescent hepatocyte in the end stage liver disease. In addition, the gene expression of the UPR^{MT} pathway was also evaluated in the chronology of events leading to cirrhosis. Extrinsic factors such as alcohol, lipid and hepatotropic viruses, are known to compromise mitochondrial functions. Hence, these etiologies were excluded and the focus of the study was on cryptogenic liver disease where there is no information available, to the best of our knowledge, on the molecular events involved in disease progression. A detailed workout on the different subject groups, their clinical and pathological characterization is described in the material and methods section. Briefly, the four groups in the study included are control subjects, fibrosis, compensated and decompensated cirrhosis. The clinical and immunohistochemical parameters of the various subjects are shown in Table 1. As expected the decompensated liver showed a significantly higher MELD score, lowered levels of albumin and deranged liver function tests.

The senescence-associated gene signature (p21, p53, γH2AX, LaminB1 and $H_3K_9Me_3$), was used to identify hepatocyte senescence in liver disease by performing immunohistochemistry on serial sections of 15 cases in each subject group of different histological stages ranging from Fibrosis (Stage 1-2) to cirrhosis (Stage 5-6 with compensated and decompensated states). A progressive increase in

staining of γH2AX in hepatocyte nuclei was noted in cirrhosis as compared to fibrosis indicative of persistent DNA damage (Fig. 5). Accumulation of p53 and p21 in cirrhotic liver, together with loss of Ki67 (Fig. 6) staining indicated growth arrest of hepatocyte. Staining of LaminB1 appeared solely on the nuclear membrane of hepatocytes in control and early fibrotic stage. Compensated cirrhotic liver showed a mixed pattern for LaminB1 expression, unchanged or with partial loss from nuclear membrane. However, LaminB1 appeared feebly stained and predominantly in nucleoplasm with either a complete or partial loss from the nuclear membrane, in decompensated cirrhotic liver. Surprisingly, the staining intensity or level of $H_3K_9me_3$ remained unaffected in the various stages of liver disease (Fig. 6). These results indicated hepatocyte senescence as a key feature of cryptogenic liver disease, and loss of LaminB1 appeared to be a promising senescence-associated marker.

Next, we tested if progression towards decompensation is also associated with mitochondrial dysfunction. Transmission electron microscopy of control liver revealed presence of multiple intact electron dense mitochondria with well formed cristae (Fig. 7A). The compensated cirrhotic liver showed mitochondria with either well defined or poorly formed cristae. The decompensated cirrhotic tissue showed enlarged mitochondria with a loss of cristae. The alterations in mitochondrial morphology in liver disease were also associated with alterations in UPR^{MT} pathway. The expressions of most UPRMT genes (CLPP, HSP60, TIM17 and NOA1) were relatively similar in control and fibrosis group. The compensated cirrhotic cases showed relatively higher RNA expression of UPR^{MT} genes (CLPP, YME1L1, HSP60 and ATF5) when compared to decompensated cirrhosis and fibrosis (Fig. 7B). Of these, mitochondrial protease, CLPP, showed the most significant increase in its transcript level in compensated cirrhosis. In immunohistochemistry also, an intense CLPP expression was noted in the compensated cirrhotic tissue, which also appeared punctate possibly indicative of its mitochondrial localization (Fig. 7C). The other UPR^{MT} markers viz. HSP60 and HSP10 also showed an increase in IHC intensity scores in compensated cirrhosis compared to both control and decompensated state (Fig. 7C). These results indicated a probable role of an activated mitochondrial stress response pathway as an adaptive response only in the compensated cirrhotic liver.

CLPP over-expression in hepatoma cells attenuates senescence by inhibiting ROS

Amongst all the UPR^{MT} genes CLPP showed maximal expression in compensated liver, hence it was over-expressed in hepatoma cells to evaluate its role in premature senescence. Both HepG2 and Huh7 cells were transfected with either CLPP-GFP or GFP alone and stable cell clones were selected showing more than 90% GFP positivity (Fig. 8A). Unlike the control cells which showed a pan GFP expression, the CLPP over-expressing cells showed a punctate pattern in the cytoplasm which co-localized with Mitotracker, thereby confirming its mitochondrial localization (Fig. 8B). The growth kinetics of CLPP over-expressing cells was similar to their control counterpart (Fig. 8C). When treated with doxorubicin, the CLPP-GFP cells showed almost 50% reduction in SA-β-Gal staining

when compared to control GFP cells (Fig. 9A,B). This was also accompanied with increased levels of LaminB1 and decreased levels of γH2AX and $H_3K_9Me_3$ in doxorubicin treated CLPP cells (Fig. 8C). Senescence is often accompanied by a secretory phenotype which was much subdued in CLPP expressing cells when exposed to doxorubicin (Fig. 9D).

Next, we examined the probable mechanisms by which CLPP could attenuate cellular senescence. Several studies have implicated reactive oxygen species (ROS) in regulating cellular senescence. To examine the mitochondrial specific ROS generation, cells were stained with MitoSOX and detected by flow cytometry. The doxorubicin treated senescent HepG2 and Huh7 cells expressing GFP alone showed higher ROS levels on 6^{th} day compared to non-senescent counterparts (Fig. 9E). However, the CLPP over-expressing cells showed a significant decline (3 fold in HepG2 and 2 fold in Huh7) in the ROS levels after Dox treatment on 6^{th} day (Fig. 9E). Besides ROS level, we also evaluated if CLPP can alter mitochondrial functioning by effecting either its number or biogenesis. Ratio of mtDNA (12S)/nDNA (18S) gene was used to quantify changes in mtDNA levels. Expression of CLPP marginally enhanced 12S/18S ratio in absence of doxorubicin stress. Intriguingly, following doxorubicin treatment both vector alone and CLPP over-expressing cells showed similar low level of mitochondrial DNA (Fig. 10A). This indicated that CLPP is not able increase the mitochondrial DNA content following stress. Multiple transcription factors play a role in mitochondrial biogenesis, of which main regulators are Peroxisome proliferator-activated receptor gamma coactivator-1 alpha (PGC-1α) and its downstream targets mitochondrial transcription factor A (TFAM) and nuclear respiratory factor (NRF1 and NRF2). CLPP on its own was unable to alter the expression levels of regulators involved in the mitochondrial biogenesis pathway in absence or presence of doxorubicin induced stress (Fig. 10B). Since mitochondrial biogenesis remained unaffected by CLPP, we next tested the possibility if CLPP can rescue the damaged mitochondria by restoring their polarization state. Over-expression of CLPP could not change the polarization status of mitochondria in both the cell lines as evident by Mitotracker staining (Fig. 10C). These results thus indicate that CLPP has little role in mitochondrial biogenesis and polarization status in conditions of stress induced premature senescence. Overall the results indicated that CLPP over-expression can reduce senescence by lowering the oxidative stress and the resulting DNA damage.

CLPP over-expression rescues senescent phenotype in non-neoplastic hepatocytes, PH5CH8

Since HepG2 and Huh7 are hepatoma cells, we repeated some of the experiments in PH5CH8 cells, which are non-neoplastic immortalised human hepatocytes and closely resembles the primary hepatocytes [21]. Doxorubicin treatment led to induction of senescence in PH5CH8 cells with almost 90% cells showing SA-β-Gal positivity (Fig. 11A). The senescent PH5CH8 cells also showed lower levels of UPR^{MT} players viz. CLPP, HSP60 and HSP10, with a significant 2 fold reduction in CLPP expression in the senescent cells when compared to the control (Fig. 11B). Hence, CLPP was

transiently transfected into PH5CH8 cells. CLPP-GFP showed a distinct punctate pattern in the cytoplasm, unlike that of pan localization pattern of GFP vector alone (Fig. 11C). Further, CLPP-GFP colocalized with Mitotracker Red confirming its mitochondrial localisation in the non-tumorigenic hepatocyte cell line (Fig. 11D). On the sixth day following treatment with doxorubicin, the CLPP over-expressing PH5CH8 showed an increase in levels of LaminB1 and decrease in levels of γH2AX and $H_3K_9Me_3$ compared to the control (Fig. 11E). However, unlike the hepatoma cells, the changes in levels of these senescent markers in PH5CH8 were not statistically significant. This in turn is explained by the fact that PH5CH8 cells are difficult to transfect with only 30% transient transfection efficiency.

Effect of CLPP on mitochondrial respiration

As CLPP is localized in mitochondria an obvious question was whether it can affect the oxygen consumption and bioenergetics profile following doxorubicin stress. The overall respiratory responses was measured using the Seahorse extracellular flux analyzer, for the hepatoma cells expressing either GFP vector or CLPP and additionally cells were treated with and without doxorubicin. The respiratory response is illustrated in Fig. 12A. In general Huh7 cells exhibited higher basal rate of respiration compared to HepG2 cells (Fig. 12A, B). Compared to control, the basal respiration rate was higher in senescent HepG2 cells; while Huh7 senescent cells showed a subtle, albeit non-significant, decrease. Similar to the extracellular flux assay, the respiratory capacity of isolated mitochondria using an oxygen microsensor (TBR1025: One-Channel Free Radical Analyzer), in presence of CLPP, was barely affected (Fig. 12E). Overall, in the absence of doxorubicin induced stress, CLPP over-expression on its own did not alter the basal respiration profile in both the hepatoma cell lines, (Fig. 12A, B, E). Following doxorubicin treatment, HepG2-CLPP showed a decrease in basal, maximal and ATP linked respiration (Fig. 12B-D) in contrast to the marked increase in treated Huh7-CLPP cells, compared to doxorubicin-treated GFP cells (Fig. 12B-D). To get an overall picture of the bioenergetics profile of CLPP over-expressing cells in presence and absence of doxorubicin-induced stress, the basal OCR vs. ECAR data was plotted (Fig. 12F). The energy map showed HepG2 having a glycolytic phenotype, while Huh7 cells showed a high metabolic phenotype with higher glycolysis and oxidative phosphorylation (OXPHOS). On its own, CLPP shifted the bioenergetic profiles in presence of doxorubicin stress, but not in its absence. Doxorubicin-treated HepG2-GFP senescent cells showed high metabolic state, while HepG2-CLPP doxorubicin treated cells showed a low glycolytic profile. Huh7-GFP Dox treated senescent cells had glycolytic phenotype whereas, Huh7-CLPP Dox treated cells showed higher energetic state of both OXPHOS and glycolysis. Overall, these results indicated that CLPP affects the mitochondrial respiration only when cells are exposed to stress conditions, and, further, it shifts the energy phenotype depending on the cellular context.

Discussion

Hepatocyte senescence resulting in growth inhibition is often a terminal event following liver injury. Strategies to prevent senescence are likely to stop end stage liver disease progression. Infact, a recent study has suggested that regenerative capacity of liver can be improved by specifically targeting the senescent hepatocytes [22]. The present study describes UPR^{MT} as a key pathway to prevent senescence-associated dysfunction. Decline in UPR^{MT} exaggerates the hepatocyte senescence and shifts the cirrhotic fate towards decompensation.

Hepatocyte senescence associated with loss of LaminB1 is a prominent feature of decompensated cryptogenic cirrhosis

Unlike the molecular events associated with alcoholic, viral and fatty liver disease etiologies, hardly any data is available on cryptogenic liver disease. The present study for the first time indicate accumulation of senescent hepatocytes in cryptogenic cirrhosis which in turn was accompanied by persistent DNA damage (γH2AX), mito-inhibition (low Ki67 index and increase in cell cycle inhibitors p21 and p53), together with loss of nuclear lamina protein LaminB1. However, it is important to note that increased levels of p53 and p21 can also help maintain quiescence in hepatocytes [23, 24] and hence more specific markers of senescence are required. We now report that loss of LaminB1 is a promising marker to detect senescent hepatocytes in liver disease. The nuclear lamins belong to class of intermediary filaments which help in maintaining the nuclear morphology, structure and function [25]. Recent studies have indicated mutations in lamin or lamin associated genes in fatty liver disorders and knockout of lamin in rodent model resulted in spontaneous fatty liver development [26, 27]. In view of a role of lamin in gastrointestinal and liver disease [28] we surmise that premature senescence-associated with loss of LaminB1, as a possible cause of cryptogenic cirrhosis.

Compensated cirrhosis mounts a strong UPR^{MT}, which is compromised in decompensated cirrhotic liver and senescent hepatocytes

The present data indicated a specific increase in UPR^{MT} pathway in compensated cirrhosis compared to both early fibrosis and late decompensated state, thereby making it important as the data is scanty regarding the molecular event(s) which help in preserving organ function during compensatory phase of cirrhosis. Using a rodent cirrhotic model Liu *et al*. [29] constructed different gene clusters in compensated vs. decompensated liver. Of these, the gene cluster with NFκB as a hub protein, showed an initial increased expression during early cirrhosis followed by a decrease in later stages. Our results on UPR^{MT} signalling is similar to the observations of Liu *et al*. as compensated cirrhotic liver mounted a strong UPR^{MT} signalling, which in contrast was attenuated in decompensated liver. In fact, the electron micrographs showed near normal mitochondria in compensated cirrhosis, thereby

indicating a possible role of UPR^{MT} in maintaining organelle integrity. This probably could explain why even in presence of senescent cells, the compensated liver could retain its function. Thus, we infer that UPR^{MT} is a compensatory mechanism mounted during early phase of cirrhosis to help maintain the hepatocyte function; however beyond a certain limit a precipitous decline in the mitochondrial stress pathway can lead to progressive phase of decompensation. While a role of hepatocyte senescence has been shown in liver disease due to alcohol, fatty liver and viral etiologies [30], it remains to be seen if the role of UPR^{MT} seen in cryptogenic cirrhosis is also applicable to other known causes of liver disease. Nonetheless, the present work indicated UPR^{MT} as a promising therapeutic target in liver disease.

Over-expression of mitochondrial protease, CLPP attenuates senescence response, reduces oxidative stress and alters the mitochondrial respiration

The contrasting difference in UPR^{MT} in compensated and decompensated cirrhotic liver led us to reason that UPR^{MT} pathway may provide a survival advantage and even protect cells from stress induced senescence. Indeed, CLPP over-expression suppressed senescence-associated markers in both the hepatoma cell lines regardless of their p53 status. Our results are also supported by a report that loss of CLPP accelerated replicative senescence in mouse fibroblasts [31]. Additionally, knockdown of CLPP in muscle cells lead to decrease in proliferation which was not due to cell death [32]. There are contradictory results on CLPP knockout and ageing. Gispert *et al*. (2013) reported that CLPP knockout mice are smaller sized and have high postnatal mortality [31]. On the contrary, yet another mouse model showed that loss of CLPP resulted in death *in utero* and those pups which survived showed normal ageing [33]. The probable mechanism by which CLPP attenuates senescence response is mostly by lowering the levels of reactive oxygen species. The mitochondrial protease complex of LON-CLPP can degrade the mitochondrial complex I ROS generating domain, thereby reducing ROS levels of the depolarized mitochondria [34]. Also, knocking out CLPP in cancerous cells resulted in increased ROS levels [35]. Since oxidative stress is a major initiator of senescence response, restoring mitochondrial protease activity may prove beneficial as an antioxidative strategy. As CLPP and other UPR^{MT} markers are upregulated in compensated liver cirrhosis, we surmise that mitochondrial retrograde response will act as an effective strategy in maintaining mitohormesis during liver injury.

We found that CLPP influenced respiration only under conditions of oxidative stress. Intriguingly, in the two cell lines tested, CLPP exerted totally opposing effects on respiration; a decrease in OCR was seen in HepG2 cells and a contrary increase was observed in Huh7 cells. In view of these confounding results, we surmise that an effect of CLPP on respiration to prevent senescence is dependent on the cellular context. Knockdown of CLPP either in muscle cell line C2C12 or in leukemic cells resulted in lower basal respiration rate [32, 35] but loss of CLPP resulted in increase in basal respiration in white

adipose tissue [18]. Following CLPP knockout, only a moderate respiratory deficiency was reported in heart cells [36]. Thus, it is inferred that effect of CLPP on respiration is dictated by not only the cellular context but also the stress incurred. The present study, notwithstanding the small number of clinical samples, highlights a role of UPR^{MT} as a potential drug target in liver disease.

Cryptogenic liver disease is generally believed to be burnt-out cases of autoimmune hepatitis (AIH), occult alcoholism and fatty liver, however, a recent study by Thuluvath et. al., indicated that cryptogenic disease is a distinct entity [37]. Whatever, may be the initial cause, the subsequent molecular events in progression of cryptogenic disease remained elusive till now. In this regard, the present study is novel, as it has unravelled a role of hepatocyte senescence together with decline in UPR^{MT} signalling as key events in development of cryptogenic liver disease. In conclusion, mounting either a strong UPR^{MT} or restoring CLPP level appears to be a promising mitohormetic strategy in not only reducing cellular senescence by preventing oxidative stress, but also augmenting hepatocyte function to prevent cirrhosis associated decompensation.

Materials and Methods:

Cell lines and reagents

HepG2 ($p53^{+/+}$) and Huh7 cells ($p53^{mut}$) were obtained from NCCS, India. PH5CH8 cells were a kind gift from Prof. Nobuyuki Kato, Okayama University Japan. All cell lines were grown in DMEM (Cell Clone-Cat#CC3004) containing 10% FBS (Hyclone-Cat#SH30071), 100mg/ml penicillin, 100mg/ml streptomycin, 2.5µg/ml Amphotericin B (Hyclone-Cat#SV30079) and 2.5mM L-glutamine at 37^0C with 5% CO_2 in a humidified incubator. Various antibodies with their dilutions and source of fluorescent dyes are given in Table 2.

Clinical samples and work out of subjects

The study included four different groups: Healthy control, Fibrosis, Compensated Cirrhosis and Decompensated Cirrhosis with 15 subjects in each group. Our hospital is a tertiary referral centre for liver diseases and in the prospective study done between 2015-2016, an average of about 733 patients with cirrhosis required admission of which 5.9% cases (43/733) were with unrecognized etiologies. These subjects tested negative for HBV-DNA and HCV- RNA. The sera of these subjects were also negative for autoantibodies thereby ruling out autoimmune disorders. Further, these subjects had no genetic/family history of liver disease and did not have history of significant alcohol consumption. Since, most of the cryptogenic cases are believed to be burnt-out NASH, in the present study, patients with histological hepatic steatosis of <5% were also included. The biopsy of all the included patients had no evidence of any other possible etiology for liver cirrhosis.

The clinical staging of cirrhosis was classified into compensated or decompensated groups based on absence or presence of any evidence of decompensation- variceal bleed, hepatic encephalopathy,

ascites, or jaundice [38]. All the cases included in the present study were received for routine diagnostic reporting in the department of Pathology. The pathological review of tissue samples and re-assessment of certain histopathological features was performed by single pathologist.

Control liver tissue was obtained from farthest, non tumour area (>2 cm) of surgically resected specimens from patients undergoing surgery for cholangiocarcinoma and showing no specific pathology of liver. For fibrosis and compensated cirrhosis, liver biopsy was obtained from patients. Diagnosis of compensated group was based on the absence of clinical criteria of decompensation. Explant cirrhotic liver tissue was collected from patients undergoing live donor liver transplant surgery and this group mainly constituted the cryptogenic decompensated group.

Fibrosis group comprised cases showing fibrous expansion of some portal areas, with or without short fibrous septa and no evidence of bridging. Histological sub-classification of cirrhosis was performed according to Laennec staging system, a modification of Metavir system [39].

Immunohistochemistry for senescence-associated markers were done in all the subjects (N=15 in each group). However, UPR^{MT} expression was studied in a subset of subjects (Control-5, Fibrosis-6, Compensated cirrhosis-8, and Decompensated cirrhosis-7) where enough material was available to do both RNA expressions by qPCR and IHC. Samples were collected after approval from institutional ethics committee (approval # F25/5/43/AC/ILBS/2013/1157) according to Helinski declaration and informed consent was taken from all the patients.

Treatment of cells with doxorubicin for induction of senescence

HepG2 and Huh7 were treated with 2µM doxorubicin (Dox, Sigma- Cat#D1515) for 2hr in complete DMEM. However, for stable cells (expressing GFP or CLPP-GFP) a lower dose of 1µM doxorubicin was used. This is because 1 µM dose was found to be sufficient for inducing senescence in both GFP control and CLPP over-expressing cells. As 2µM dose of doxorubicin also resulted in cell death in stable cells, hence to delineate effects specific to senescence, the lower dose of doxorubicin was preferred. Cells were washed once and then replenished with media containing 10% FBS. Medium was changed on 3rd day. Induction of senescence on 6th day was confirmed by Senescence associated-β-Galactosidase assay as previously described by Dimri *et al*., [40]. Briefly, cells were fixed with 2% formaldehyde and 0.2% glutaraldehyde in PBS, and then washed with PBS. Cells were stained for 3 h to 24 h in X-gal staining solution [1 mg/ml X-gal, 40 mM citric acid/sodium phosphate (pH 6.0), 5 mM potassium ferricyanide, 5 mM potassium ferrocyanide, 150 mM NaCl, 2 mM $MgCl_2$] at 37^{0}C in a non-CO_2 incubator. Cell stained with characteristic blue color were identified and counted using bright field microscopy.

Growth assay by crystal violet

10,000 cells were plated in 24 well plates in triplicates and treated with doxorubicin the following day. Cells were stained with 0.2% crystal violet made in 2% ethanol at indicated time intervals after doxorubicin treatment and collected in 1% SDS. The absorbance was recorded at 570nm.

Cell cycle analysis by flow cytometry

Cells were fixed in 70% ethanol, washed, stained with propidium iodide solution containing 5mg/ml RNase A at 37^0C in dark and acquired in a flow cytometer (BD FACSCalibur™, BD Biosciences, San Jose, CA) and DNA content was measured at 630/22 nm filter. Data analysis was done by FlowJo® software (Beckton-Dickenson, USA).

Immunofluorescence imaging

Cells plated on coverslips were fixed with either methanol/acetone (1:1) or 4% formaldehyde in PBS. Blocking and permeabilization was done in 3% BSA containing 0.1% Triton X-100 followed by incubation with primary antibody diluted in 1% BSA overnight at 4^0C. Primary antibody was detected using Alexa Fluor 488 or 594 conjugated secondary (anti-mouse/rabbit/goat) antibodies and mounted in DAPI mounting media. Images were taken either with confocal microscope (LEICA TCS SP2 Confocal Laser Scanning Microscope, Leica Microsystems, Heidelberg, Germany) or a fluorescence microscope (Nikon ECLIPSE Ni, Nikon Instruments Inc., Melville, NY). MFI of confocal images were calculated using LAS AF Lite software, Leica Microsystems.

Immunoblotting

Cells were lysed in RIPA lysis buffer containing protease inhibitors (1mM PMSF, 1mg/ml aprotinin) and phosphatase inhibitors (1mM sodium orthovanadate, 10mM sodium fluoride). Equal amount of protein was separated onto 12% SDS-polyacrylamide gels and transferred to PVDF membrane. Blots were blocked in 5% non-fat dry milk, incubated with respective primary antibodies followed by incubation with HRP-conjugated secondary antibody. Single blot was cut and probed for different antibodies. The signals were detected by Clarity Max Western ECL substrate (Bio-Rad, Hercules, CA) using chemiluminescence detection system (Proteinsimple, San Jose, CA). Quantification of immunoblots was done using Image J software (NIH, Bethesda, MD).

RNA extraction and quantitative Real-Time Polymerase Chain Reaction (qPCR)

RNA was extracted from cell lines and tissue samples using TRIzol (Cat#15596018-Invitrogen, Carlsbad, CA) method according to manufacturer's protocol. cDNA was synthesized from 1µg RNA using RevertAid First Strand cDNA Synthesis Kit (Cat#K1622-Thermo Scientific, Waltham, MA). qPCR was performed using Maxima SYBR Green (Cat#K0222-Thermo Scientific) in ABI ViiA 7 detection system (Applied Biosystems, Foster City, CA). Gene expression was normalised against

18S mRNA which served as an internal control. Relative expression was calculated using the formula $2^{-\Delta\Delta Ct}$ [41].

Mitochondrial polarization and mitochondrial ROS detection

For mitochondrial polarisation, cells were trypsinized, washed with PBS and stained with 100nM Tetramethylrhodamine ethyl ester (TMRE) in PBS containing 1% FBS for 20-30min at 37^0C in dark. After incubation, cells were washed twice with staining buffer (PBS, 1% FBS) and acquired in BD FACSVerse™ (BD Biosciences, San Jose, CA). For imaging, cells were stained with 100nM MitoTracker in staining buffer for 30min at 37^0C, washed and fixed in 4% formaldehyde for 15min. Images were taken in fluorescence microscope. For estimating mitochondrial ROS, cells were suspended in staining buffer containing 5µM MitoSOX for 10min at 37^0C in dark, washed and acquired in BD FACSVerse™. Data was analysed on GFP+ gated population using FlowJo® software.

Transmission electron microscopy

4 X 10^6 cells (N=3 for each sample) or $1mm^3$ for tissue (2 specimen from each subject) were fixed with 2.5% glutaraldehyde and 2% paraformaldehyde, made in 0.1M sodium phosphate buffer (pH 7.4) overnight at 4^0C. Secondary fixation was done in 1% osmium tetroxide. Fixed cells were dehydrated in various grades of acetone followed by clearing with toluene and infiltration with decreasing toluene: resin ratios. Blocks were prepared in epoxy resin. From each block 3 ultrathin sections were mounted onto copper grids and viewed on high resolution transmission electron microscope**,** TECNAI 200 Kv TEM (Fei, Electron Optics, Hillsboro, OR). Atleast 5-10 random areas were chosen for viewing from each section.

Immunocytochemistry for Ki67

Control and doxorubicin treated cells grown on coverslips were serum stimulated for 24hr followed by fixation in 4% formaldehyde. Cells were blocked and permeabilised in 3% BSA containing 0.1% Triton X-100 for 1 hr and incubated with Ki67 antibody overnight at 4^0C. This in turn was detected by HRP-labelled secondary antibody using DAB (3, 3′ Diaminobenzidine) (Cat# QD420-YIKE BioGenex, Fremont, CA) for colour development.

Immunohistochemistry

Formalin fixed paraffin embedded tissue sections (4µM) were deparaffinised in xylene and rehydrated in decreasing grades of ethanol. Tissue sections were blocked in 3% H_2O_2 for 10min followed by antigen retrieval in either citrate buffer (pH 6) or Tris-EDTA buffer (pH 9). Power block was performed using BioGenex kit for 5min. Slides were incubated with primary antibody overnight at 4^0C followed by treatment with Super Enhancer (Cat# QD420-YIKE BioGenex, Fremont, CA) for 20min. This was then detected by incubation with HRP tagged antibody followed by colour

development using DAB as chromogen. Hepatocytes were distinguished based on size and polygonal shape, further the cord arrangement of the hepatocytes as evident in the images also helped in delineating them from the other cell types present in the portal and sinusoidal area. Stained slides were photographed in bright field microscope (Nikon ECLIPSE Ni, Nikon Instruments Inc.) and evaluated by a pathologist based on % positivity (positive cells/total cells X 100) and staining intensity (0-absent, 1-minimal, 2-moderate, 3-severe). IHC scores were calculated as % positivity X intensity.

Plasmid constructs, transfection and generation of stable cell clones

Full length human CLPP cDNA was cloned in pEGFP-N1 at XhoI and BamHI sites. pEGFP-N1 empty backbone was used as control. GFP and CLPP-GFP plasmids were transfected in HepG2, Huh7 and PCH5CH8 cells using Lipofectamine® LTX with Plus™ Reagent (Cat#15338100, Invitrogen, Carlsbad, CA). These cells were selected and cultured in presence of Geneticin (500µg/ml; Cat#10131027, Gibco™, Carlsbad, CA). Stable cell lines of HepG2 and Huh7 were established by dilution plating. Percentage of GFP+ cells were evaluated by flow cytometry.

Mitochondrial DNA estimation

To estimate mitochondrial DNA depletion, genomic DNA was isolated using phenol/chloroform/isoamylalcohol. mtDNA copy number was determined by co-amplifying mitochondria encoding 12S rRNA and nuclear encoding 18S rRNA as reference gene. SYBR green chemistry was used for qPCR amplification.

Mitochondria isolation and oxygen consumption rate

Mitochondria were isolated from $20X10^6$ cultured cells using Mitochondria Isolation Kit (Cat #89874, Thermo Fisher Scientific Waltham, MA) according to the manufacturer's protocol. The isolated mitochondrial fraction was resuspended in suspension buffer [HEPES (20mM, pH 7.2), sucrose (0.3M), EDTA (1mM), $MgCl_2$ (2mM), KH_2PO_4 (0.5mM)] and the change in dissolved oxygen concentration was monitored every 30sec by using TBR1025 single-channel free radical analyzer (World Precision Instruments, Sarasota, FL).

Mitochondrial stress test

Oxygen consumption rate (OCR) and extracellular acidification rate (ECAR) was analysed using Seahorse XF24 Analyzer and Seahorse XF Cell Mito Stress Test Kit (Cat#103015, Agilent/Seahorse Bioscience, Santa Clara, CA). FCCP concentration and cell density was standardised prior to experiment setup. Sensor cartridge was hydrated and equal numbers of cells were seeded onto Seahorse XF24 Cell Culture Microplates one day before assay. On the day of assay the cartridge was loaded with oligomycin (10µM), FCCP (5µM for HepG2 and 2.5µM for Huh7) and

rotenone/antimycin A (5μM). The compounds were serially injected to measure the basal and the changes in OCR after addition of the electron transport chain inhibitors. After the end of the assay, total protein content in each well was quantified by BCA Protein Assay Kit (Cat#23225; Thermo Scientific, Waltham, MA) and was used to normalise the OCR values.

Statistics

All statistical analysis were done using GraphPad Prism version 6.01 for Windows, GraphPad Software, La Jolla, CA, www.graphpad.com. Two tailed Student's t-test was used for cell culture experiments to arrive at the p values between two different conditions. For clinical samples, Kruskal Wallis one-way ANOVA with Dunn's multiple comparison tests was used to calculate p values between the groups. Differences were considered statistically significant with p values less than 0.05 (* $P \leq 0.05$, ** $P \leq 0.01$, *** $P \leq 0.001$, **** $P \leq 0.0001$). Data was represented as mean ± SD from biological replicates.

Acknowledgments:

We thank Prof. T Ramasarma and Dr. Lucy Anderson for critical reading and editing of the manuscript. BS is a recipient of UGC senior research fellowship. We thank Dr. Nobuyuki Kato, Okayama University for providing us the PH5CH8 cells. We thank DST-FIST for support. We also thank the anonymous reviewers for their valuable inputs.

References:

[1] Tsochatzis EA, Bosch J, Burroughs AK. Liver cirrhosis. Lancet 2014;383(9930):1749-61.

[2] Aravinthan A, Pietrosi G, Hoare M, Jupp J, Marshall A, Verrill C, Davies S, Bateman A, Sheron N, Allison M, Alexander GJ. Hepatocyte expression of the senescence marker p21 is linked to fibrosis and an adverse liver-related outcome in alcohol-related liver disease. PloS one 2013;8(9):e72904.

[3] Paradis V, Youssef N, Dargere D, Ba N, Bonvoust F, Deschatrette J, Bedossa P. Replicative senescence in normal liver, chronic hepatitis C, and hepatocellular carcinomas. Human pathology 2001;32(3):327-32.

[4] Aravinthan A, Scarpini C, Tachtatzis P, Verma S, Penrhyn-Lowe S, Harvey R, Davies SE, Allison M, Coleman N, Alexander G. Hepatocyte senescence predicts progression in non-alcohol-related fatty liver disease. Journal of hepatology 2013;58(3):549-56.

[5] Dooley S, ten Dijke P. TGF-beta in progression of liver disease. Cell and tissue research 2012;347(1):245-56.

[6] Hoare M, Das T, Alexander G. Ageing, telomeres, senescence, and liver injury. Journal of hepatology 2010;53(5):950-61.

[7] Jiang H, Ju Z, Rudolph KL. Telomere shortening and ageing. Zeitschrift fur Gerontologie und Geriatrie 2007;40(5):314-24.

[8] Natarajan SK, Thomas S, Ramamoorthy P, Basivireddy J, Pulimood AB, Ramachandran A, Balasubramanian KA. Oxidative stress in the development of liver cirrhosis: a comparison of

two different experimental models. Journal of gastroenterology and hepatology 2006;21(6):947-57.

[9] Reyes-Gordillo K, Shah R, Muriel P. Oxidative Stress and Inflammation in Hepatic Diseases: Current and Future Therapy. Oxidative medicine and cellular longevity 2017;2017:3140673.

[10] Shimura T, Sasatani M, Kamiya K, Kawai H, Inaba Y, Kunugita N. Mitochondrial reactive oxygen species perturb AKT/cyclin D1 cell cycle signaling via oxidative inactivation of PP2A in lowdose irradiated human fibroblasts. Oncotarget 2016;7(3):3559-70.

[11] Grattagliano I, Russmann S, Diogo C, Bonfrate L, Oliveira PJ, Wang DQ, Portincasa P. Mitochondria in chronic liver disease. Current drug targets 2011;12(6):879-93.

[12] Hoshino A, Mita Y, Okawa Y, Ariyoshi M, Iwai-Kanai E, Ueyama T, Ikeda K, Ogata T, Matoba S. Cytosolic p53 inhibits Parkin-mediated mitophagy and promotes mitochondrial dysfunction in the mouse heart. Nature communications 2013;4:2308.

[13] Pang L, Liu K, Liu D, Lv F, Zang Y, Xie F, Yin J, Shi Y, Wang Y, Chen D. Differential effects of reticulophagy and mitophagy on nonalcoholic fatty liver disease. Cell death & disease 2018;9(2):90.

[14] Williams JA, Ding WX. A Mechanistic Review of Mitophagy and Its Role in Protection against Alcoholic Liver Disease. Biomolecules 2015;5(4):2619-42.

[15] Shpilka T, Haynes CM. The mitochondrial UPR: mechanisms, physiological functions and implications in ageing. Nature reviews Molecular cell biology 2018;19(2):109-20.

[16] Schulz AM, Haynes CM. UPR(mt)-mediated cytoprotection and organismal aging. Biochimica et biophysica acta 2015;1847(11):1448-56.

[17] Gariani K, Menzies KJ, Ryu D, Wegner CJ, Wang X, Ropelle ER, Moullan N, Zhang H, Perino A, Lemos V, Kim B, Park YK, Piersigilli A, Pham TX, Yang Y, Ku CS, Koo SI, Fomitchova A, Canto C, Schoonjans K, Sauve AA, Lee JY, Auwerx J. Eliciting the mitochondrial unfolded protein response by nicotinamide adenine dinucleotide repletion reverses fatty liver disease in mice. Hepatology 2016;63(4):1190-204.

[18] Bhaskaran S, Pharaoh G, Ranjit R, Murphy A, Matsuzaki S, Nair BC, Forbes B, Gispert S, Auburger G, Humphries KM, Kinter M, Griffin TM, Deepa SS. Loss of mitochondrial protease ClpP protects mice from diet-induced obesity and insulin resistance. EMBO reports 2018;19(3).

[19] Becker C, Kukat A, Szczepanowska K, Hermans S, Senft K, Brandscheid CP, Maiti P, Trifunovic A. CLPP deficiency protects against metabolic syndrome but hinders adaptive thermogenesis. EMBO reports 2018;19(5).

[20] Anwar T, Khosla S, Ramakrishna G. Increased expression of SIRT2 is a novel marker of cellular senescence and is dependent on wild type p53 status. Cell cycle 2016;15(14):1883-97.

[21] Kato N, Ikeda M, Sugiyama K, Mizutani T, Tanaka T, Shimotohno K. Hepatitis C virus population dynamics in human lymphocytes and hepatocytes infected in vitro. The Journal of general virology 1998;79 (Pt 8):1859-69.

[22] Bird TG, Muller M, Boulter L, Vincent DF, Ridgway RA, Lopez-Guadamillas E, Lu WY, Jamieson T, Govaere O, Campbell AD, Ferreira-Gonzalez S, Cole AM, Hay T, Simpson KJ, Clark W, Hedley A, Clarke M, Gentaz P, Nixon C, Bryce S, Kiourtis C, Sprangers J, Nibbs RJB, Van Rooijen N, Bartholin L, McGreal SR, Apte U, Barry ST, Iredale JP, Clarke AR, Serrano M, Roskams TA, Sansom OJ, Forbes SJ. TGFbeta inhibition restores a regenerative response in acute liver injury by suppressing paracrine senescence. Science translational medicine 2018;10(454).

[23] Kwon YH, Jovanovic A, Serfas MS, Kiyokawa H, Tyner AL. P21 functions to maintain quiescence of p27-deficient hepatocytes. The Journal of biological chemistry 2002;277(44):41417-22.

[24] Inoue Y, Tomiya T, Nishikawa T, Ohtomo N, Tanoue Y, Ikeda H, Koike K. Induction of p53-dependent p21 limits proliferative activity of rat hepatocytes in the presence of hepatocyte growth factor. PloS one 2013;8(11):e78346.

[25] Dechat T, Pfleghaar K, Sengupta K, Shimi T, Shumaker DK, Solimando L, Goldman RD. Nuclear lamins: major factors in the structural organization and function of the nucleus and chromatin. Genes & development 2008;22(7):832-53.

[26] Kwan R, Brady GF, Brzozowski M, Weerasinghe SV, Martin H, Park MJ, Brunt MJ, Menon RK, Tong X, Yin L, Stewart CL, Omary MB. Hepatocyte-Specific Deletion of Mouse Lamin A/C Leads to Male-Selective Steatohepatitis. Cellular and molecular gastroenterology and hepatology 2017;4(3):365-83.

[27] Hendrikx T, Schnabl B. Lamin Deficiency in the Liver Sets the Stage for Nonalcoholic Steatohepatitis Development in Males. Cellular and molecular gastroenterology and hepatology 2017;4(3):441-2.

[28] Brady GF, Kwan R, Bragazzi Cunha J, Elenbaas JS, Omary MB. Lamins and Lamin-Associated Proteins in Gastrointestinal Health and Disease. Gastroenterology 2018;154(6):1602-19 e1.

[29] Liu L, Yannam GR, Nishikawa T, Yamamoto T, Basma H, Ito R, Nagaya M, Dutta-Moscato J, Stolz DB, Duan F, Kaestner KH, Vodovotz Y, Soto-Gutierrez A, Fox IJ. The microenvironment in hepatocyte regeneration and function in rats with advanced cirrhosis. Hepatology 2012;55(5):1529-39.

[30] Aravinthan AD, Alexander GJM. Senescence in chronic liver disease: Is the future in aging? Journal of hepatology 2016;65(4):825-34.

[31] Gispert S, Parganlija D, Klinkenberg M, Drose S, Wittig I, Mittelbronn M, Grzmil P, Koob S, Hamann A, Walter M, Buchel F, Adler T, Hrabe de Angelis M, Busch DH, Zell A, Reichert AS, Brandt U, Osiewacz HD, Jendrach M, Auburger G. Loss of mitochondrial peptidase Clpp leads to infertility, hearing loss plus growth retardation via accumulation of CLPX, mtDNA and inflammatory factors. Human molecular genetics 2013;22(24):4871-87.

[32] Deepa SS, Bhaskaran S, Ranjit R, Qaisar R, Nair BC, Liu Y, Walsh ME, Fok WC, Van Remmen H. Down-regulation of the mitochondrial matrix peptidase ClpP in muscle cells causes mitochondrial dysfunction and decreases cell proliferation. Free radical biology & medicine 2016;91:281-92.

[33] Szczepanowska K, Maiti P, Kukat A, Hofsetz E, Nolte H, Senft K, Becker C, Ruzzenente B, Hornig-Do HT, Wibom R, Wiesner RJ, Kruger M, Trifunovic A. CLPP coordinates mitoribosomal assembly through the regulation of ERAL1 levels. The EMBO journal 2016;35(23):2566-83.

[34] Pryde KR, Taanman JW, Schapira AH. A LON-ClpP Proteolytic Axis Degrades Complex I to Extinguish ROS Production in Depolarized Mitochondria. Cell reports 2016;17(10):2522-31.

[35] Cole A, Wang Z, Coyaud E, Voisin V, Gronda M, Jitkova Y, Mattson R, Hurren R, Babovic S, Maclean N, Restall I, Wang X, Jeyaraju DV, Sukhai MA, Prabha S, Bashir S, Ramakrishnan A, Leung E, Qia YH, Zhang N, Combes KR, Ketela T, Lin F, Houry WA, Aman A, Al-Awar R, Zheng W, Wienholds E, Xu CJ, Dick J, Wang JC, Moffat J, Minden MD, Eaves CJ, Bader GD, Hao Z, Kornblau SM, Raught B, Schimmer AD. Inhibition of the Mitochondrial Protease ClpP as a Therapeutic Strategy for Human Acute Myeloid Leukemia. Cancer cell 2015;27(6):864-76.

[36] Seiferling D, Szczepanowska K, Becker C, Senft K, Hermans S, Maiti P, Konig T, Kukat A, Trifunovic A. Loss of CLPP alleviates mitochondrial cardiomyopathy without affecting the mammalian UPRmt. EMBO reports 2016;17(7):953-64.

[37] Thuluvath PJ, Kantsevoy S, Thuluvath AJ, Savva Y. Is cryptogenic cirrhosis different from NASH cirrhosis? Journal of hepatology 2018;68(3):519-25.

[38] de Franchis R. Evolving consensus in portal hypertension. Report of the Baveno IV consensus workshop on methodology of diagnosis and therapy in portal hypertension. Journal of hepatology 2005;43(1):167-76.

[39] Rastogi A, Maiwall R, Bihari C, Ahuja A, Kumar A, Singh T, Wani ZA, Sarin SK. Cirrhosis histology and Laennec staging system correlate with high portal pressure. Histopathology 2013;62(5):731-41.

[40] Dimri GP, Lee X, Basile G, Acosta M, Scott G, Roskelley C, Medrano EE, Linskens M, Rubelj I, Pereira-Smith O, et al. A biomarker that identifies senescent human cells in culture and in aging skin in vivo. Proceedings of the National Academy of Sciences of the United States of America 1995;92(20):9363-7.

[41] Livak KJ, Schmittgen TD. Analysis of relative gene expression data using real-time quantitative PCR and the 2(-Delta Delta C(T)) Method. Methods 2001;25(4):402-8.

Figure Legends

Figure 1. Doxorubicin induces growth arrest in hepatoma cells.

(A) Growth curve of hepatoma cells (Huh7 and HepG2) treated with 2µM doxorubicin (Dox) for 2 hr (Day 0), replenished with fresh medium and growth kinetics was monitored at specified time intervals (1 to 6 days) by staining with crystal violet dye whose absorbance was checked spectrophotometrically at 570nm. Cells treated with vehicle alone served as control (Con). (B) Cell cycle distribution of control (Con) and doxorubicin (Dox) treated cells as analyzed by flow cytometry. Following treatment with doxorubicin for 2hr, cells were cultured for 6 days, fixed in ethanol, stained with Propidium Iodide (PI) and subjected to flow cytometry for cell cycle analysis. Representative histogram and bar graph shows the distribution of cells in different phase of cell cycle. The data shown are mean ± SD from three separate experiments. (C) Immunocytochemsitry for Ki67 in HepG2 and Huh7 control and doxorubicin treated cells after 6 days. Serum stimulation was done for 24hr prior to Ki67 staining. Inset shows magnified view of cells. Brown colour indicates Ki67 positive nuclei. Scale bars: 50µm. (D) Bar diagram showing percentage Ki67 positivity in control (Con) and doxorubicin (Dox) treated hepatoma cells. Individual data points represent percentage positivity of atleast ten different microscopic fields and data is represented as mean ± SD. Student's t test was used to calculate the significance (****, $P \leq 0.0001$)

Figure 2. Doxorubicin induces premature senescence in both HepG2 and Huh7 irrespective of their different p53 status.

(A) Bright field microscopy images of Control (Con) and Doxorubicin (Dox) treated hepatoma cells (HepG2 with wild type p53 and Huh7 with mutant p53) subjected to SA-β-galactosidase assay. Briefly, cells were treated for 2 hours with doxorubicin, changed with fresh medium and cultured for 6 days following which SA-β-galactosidase assay was done. Blue colour indicates SA-β-gal positive cells. Scale bar: 50µm. Adjoining bar diagram shows percentage SA-β-galactosidase positivity in control and doxorubicin treated cells. Individual data points represent mean percentage positivity of atleast five different microscopic view-fields. The data is represented mean ± SD of multiple replicates. (B) Representative immunoblots showing expression of senescence-associated markers viz. p21, γH2AX, $H_3K_9me_3$ and LaminB1 in control (Con) and doxorubicin (Dox) treated cells at 6th day.

(C) Bar diagrams showing the relative expression of senescence markers in control and doxorubicin treated cells normalised with GAPDH. Experiment was done in quadruplicates and data was plotted as mean ± SD. (D) Merged confocal images showing expression of γH2AX (red), $H_3K_9me_3$ (green) and LaminB1 (red) in control and doxorubicin treated cells on 6^{th} day. Cells were counterstained with DAPI (blue). (E) Bar graphs show the relative mean fluorescent intensity (MFI) of senescence-associated markers calculated in different view-fields. Individual data points represent MFI quantification in one particular field. Data represented as mean ± SD. For all the experiments described, the significance was calculated by Student's t test (* P≤0.05, ** P≤0.01, *** P≤0.001, **** P≤0.0001).

Figure 3. Mitochondrial dysfunction following senescence in HepG2 and Huh7 cells.

(A) Representative transmission electron micrographs of control and senescent hepatoma cells. Abbreviations, N: nucleus, M: mitochondria, ER: endoplasmic reticulum, AV: autophagic vacuole, *: heterochromatin. Scale bar: 1µm. (B) Representative histogram plots showing changes in mitochondrial polarization as measured by sequestration of TMRE in control (Con) and senescent (Sen) cells on 6th day as analysed by flow cytometry. Bar diagrams shows quantification of TMRE in control and senescent hepatoma cells using three biological replicates. (C) Representative images of control and senescent cells stained with mitochondrial potential dependent dye, Mitotracker Red (mitochondria, red) and counterstained with DAPI (nucleus, blue). Scale bar: 100µM and 50µM. (D) Bar diagram showing quantification of mitochondrial ROS production in control and senescent cells stained with fluorescent dye, MitoSOX, which is a probe to detect mitochondrial superoxide. (E) Mitochondrial DNA (mtDNA) quantification in HepG2 and Huh7 cells by real time qPCR amplification of mitochondrial encoded 12S rRNA and the nuclear encoded 18S rRNA which served as a reference gene. Results are expressed as relative ratio of 12S mtDNA over 18S nDNA. (F) Relative gene expression, by qPCR, of mitochondrial biogenesis regulatory genes in control vs. senescent HepG2 and Huh7 cells. For all experiments the bar indicates values as mean ± SD of three independent experiments. P values were calculated by paired student's t test (* P≤0.05, ** P≤0.01, ***P≤0.001).

Figure 4. UPR^{MT} is compromised in doxorubicin induced senescent cells.

(A) Bar graphs represent relative expression of UPR^{MT} genes as measured by real time qPCR in control vs. senescent HepG2 and Huh7 cells. The bars represent mean ± SD from three independent experiments. (B) Representative immunoblots of UPR^{MT} genes in control and senescent HepG2 and Huh7 cells. The adjoining bar graph shows their relative quantification normalised to GAPDH. Data is represented as mean ± SD of four biological replicates. P values were calculated by paired Student's t test (* P≤0.05, ** P≤0.01, ***P≤0.001, ****P≤0.0001).

Figure 5. Accumulation of senescent hepatocytes in various stages of liver disease.

Immunohistochemistry (IHC) showing senescence-associated markers in different subject groups viz., Control, Fibrosis, Compensated (Comp) Cirrhosis and Decompensated (Decomp) Cirrhosis. A total of 15 different samples were analysed in each group. Representative images show expression of DNA damage associated marker, γH2AX; growth arrest marker, p53; cyclin dependent kinase inhibitor, p21 and nuclear lamina protein, LaminB1. Brown staining indicates positivity. Scale bar: 10µM. Adjacent scatter plots show the changes in expression of each of the markers in different stages of liver disease. For γH2AX and p21, IHC score was calculated as explained in methods section. For p53, percentage positivity was plotted, whereas for LaminB1, percentage of cells with intact nuclear membrane was taken as variable for quantification. Individual data point in the scatter plot represent samples scored in each group. The quantified data is represented as mean ± SD. Kruskal Wallis one-way ANOVA with Dunn's multiple comparison test was used in order to determine the statistical significance between the groups (* P≤0.05, ** P≤0.01, ***P≤0.001, ****P≤0.0001).

Figure 6. Representative images of $H_3K_9me_3$ and Ki67 immunohistochemistry done in various subject groups viz., control, fibrosis, compensated and decompensated cirrhosis. Brown colour indicated positivity. Scale bar: 20µm.

Figure 7. Mitochondrial associated changes in various stages of end stage liver disease.

(A) Representative transmission electron micrograph of liver tissue from control, compensated and decompensated cirrhosis. Note the presence of intact electron dense mitochondrial cristae (indicated by yellow arrowheads) in control and compensated cirrhosis, while enlarged mitochondria with diffused cristae (indicated by red arrowheads) in decompensated cirrhosis. N: nucleus, ER: Endoplasmic Reticulum, H: Heterochromatin. Scale bar: 0.5µM. (B) Bar graph shows the relative expression of UPR^{MT} genes quantified by qPCR in control, fibrosis, compensated (Comp) and decompensated (Decomp) cirrhosis. Values are represented as mean ± SD. Individual data points represent number (N) of subjects in each group: N=5 in control, N=6 in fibrosis, N=8 in compensated cirrhosis and N=7 in decompensated cirrhosis. Kruskal Wallis one-way ANOVA was used to calculate the significance within the groups. (C) Representative images of liver sections showing immunohistochemistry for UPR^{MT} markers in control, fibrosis, compensated (Comp) and decompensated (Decomp) cirrhosis. Scale bar: 10µM. Adjacent scatter plots representing variations in intensity scores (0-absent, 1-minimal, 2-moderate, 3-severe) of CLPP, HSP60 and HSP10. Data is represented as mean ± SD. Kruskal Wallis one-way ANOVA with Dunn's multiple comparison test was used to calculate the significance between the groups. (*P≤0.05, **P≤0.01, ***P≤0.001, ****P≤0.0001)

Figure 8. CLPP over-expression and establishment of stable hepatoma cell lines.

(A) Histogram plots showing percentage of GFP positivity in stable HepG2 and Huh7 cells expressing either empty GFP vector or CLPP-GFP as analysed by flow cytometry. (B) Immunofluorescence images of stable cell clones of HepG2 and Huh7 cells showing expression of either GFP or CLPP-CLPP (green). Note CLPP-GFP showed a punctate expression which co-localized with Mitotracker Red. Nucleus was counterstained with DAPI. (C) Growth of cells expressing GFP and CLPP-GFP was monitored by uptake of crystal violet dye at specified time intervals and quantified by reading the absorbance at 570nm. The data is represented as mean ± SD from three independent experiments.

Figure 9. CLPP over-expression attenuated senescence-associated changes in hepatoma cells following doxorubicin treatment by reducing ROS levels.

(A) Representative bright field microscopic images of SA-β-Gal staining in GFP vector and CLPP-GFP over-expressing HepG2 and Huh7 cells following doxorubicin treatment on 6th day. Scale bar: 50µm. (B) Bar diagrams showing percentage of SA–β-Gal positive cells. Individual data points represent percentage positivity per microscopic field. (C) Immunoblots showing the expression of three senescence-associated markers and GAPDH served as loading control. The numbers below the blots represent relative fold change compared to untreated control (Con) in GFP and CLPP over-expressing cells following doxorubicin (Dox) treatment at 6^{th} day. (D) Relative expression of senescence associated secretory phenotype (SASP) markers as quantified by real time qPCR in control (Con) and doxorubicin (Dox) treated HepG2 and Huh7 cells expressing either GFP or CLPP-GFP. The data represents mean ± SD from three independent experiments. (E) Representative histogram showing shift in median fluorescent intensity (MFI) of MitoSOX which is an indicator of the mitochondrial ROS levels. The bar diagram showing quantification of mitochondrial ROS in HepG2 and Huh7 cells expressing either GFP or CLPP-GFP when treated with either vehicle or doxorubicin. MFI of MitoSOX was calculated on GFP+ gated population. Individual data points represent three biological replicates and data is represented as mean ± SD. For all statistical significance, P values were calculated by Student's t test (*P≤0.05, **P≤0.01, ***P≤0.001, ****P≤0.0001)

Figure 10. Effect of CLPP on mitochondrial DNA content, biogenesis and polarization in HepG2 and Huh7 cells.

(A) mtDNA quantification in hepatoma cells expressing either GFP or CLPP and treated without (Con) or with doxorubicin (Dox). Quantification was done by real time qPCR amplification of mitochondrial 12S rRNA gene and nuclear 18S rRNA which served as a reference gene. Results are expressed as ratio of 12S mtDNA to 18S nDNA. (B) Relative gene expression of mitochondrial biogenesis regulatory genes by real time qPCR in GFP vs. CLPP over-expressing cells treated with doxorubicin (Dox). Untreated cells served as control (Con). The bar diagram represent values plotted

as mean ± SD from three different experiments. P values were calculated by paired Student's t test (* P≤0.05, ** P≤0.01, ***P≤0.001). (C) Representative fluorescence images of control and doxorubicin (Dox) treated GFP and CLPP-GFP (green) over-expressing cells, stained with Mitotracker (mitochondria, red) dye which detects mitochondrial polarization status. Cells were counterstained with DAPI (nucleus, blue). Scale bar: 100µm, 50µm.

Figure 11. CLPP over-expression rescues senescent phenotype in non-neoplastic hepatocytes (PH5CH8).

(A) Representative bright field microscopy images of SA-β-Gal staining in control (Con) and doxorubicin (Dox, 2µM) treated cells. Cells were treated for 2hr, changed to fresh medium and grown for 6 days following which staining was done. Scale bar: 50µm. Adjoining bar diagram shows percentage SA-β-Gal positivity with data points representing atleast 10 different microscopic fields. (B) Representative immunoblots of UPR^{MT} genes in control (Con) and senescent (Sen) PH5CH8 cells. The adjoining bar graphs shows their relative quantification normalised to GAPDH. Individual data points represent three biological replicates. (C) Representative fluorescence images showing expression of GFP and CLPP-GFP (green) transiently transfected in PH5CH8 cells. Nucleus was counterstained with DAPI (blue). Scale bar 20µM. (D) Immunofluorescence images of PH5CH8 cells showing expression of either empty GFP vector or CLPP (green). As compared to pan expression of GFP vector control, CLPP showed a punctate expression which co-localized with Mitotracker Red. Nucleus was counterstained with DAPI (blue). Scale bar 10µM. (E) Representative immunoblots of senescence-associated markers in GFP and CLPP-GFP over-expressing PH5CH8 cells after doxorubicin (Dox) treatment. The adjoining bar graph shows the relative quantification normalised to GAPDH. Individual data points represent three biological replicates. The bar diagrams represent data values as mean ± SD. P values were calculated by Student's t test (* P≤0.05, ****P≤0.0001)

Figure 12. CLPP over-expression altered mitochondrial respiration in hepatoma cells.

(A) Representative Extracellular Flux Assay plots of HepG2 and Huh7 cells, expressing either GFP or CLPP, using the Seahorse XF Cell Mito Stress Test Kit. Respiration was monitored on 6th day following treatment with either doxorubicin (Dox) or vehicle (Con). The oxygen consumption rate (OCR) was monitored at basal level in the absence of exogenous substrate, followed by sequential addition of oligomycin (1.0µM), FCCP (0.50µM for HepG2 and 0.25µM for Huh7) and rotenone/antimycin A (0.5µM). Points represent mean ± SD. Protein content of each well was used to normalise the OCR. (B) Bar graphs represent basal respiration in both HepG2 and Huh7 cells expressing either GFP or CLPP. (C) Bar graphs represents maximal respiration in both HepG2 and Huh7 cells expressing either GFP or CLPP. (D) Bar graphs represent ATP linked respiration in both HepG2 and Huh7 cells expressing either GFP or CLPP. (E) Oxygen consumption rate of isolated

mitochondria from GFP and CLPP over-expressing HepG2 and Huh7 cells as measured by oxygen microsensor (TBR1025 single-channel free radical analyzer). 2mM NADH was added (arrow) after 5min and its oxidation was monitored every 30sec. (F) Energy phenotype analysis by plotting OCR vs. ECAR (extracellular acidification rate) in CLPP and GFP over-expressing cells with or without doxorubicin (Dox) treatment. The bar graph represents value as mean ± SD and P values was calculated by Student's t test (* $P \leq 0.05$, ** $P \leq 0.001$).

Table 1. Clinical parameters and immunohistochemical scores of various markers in different patient groups

Variables	Control	Fibrosis	Compensated Cirrhosis	Decompensated Cirrhosis	p value (1 way ANOVA)
Age (years)	26.20±0.58	34.00±5.77	55.75±1.81	45.57±3.85	**0.0017**
Sex (%, female)	0.60	0.33	0.50	0.29	
Total Bilirubin (mg/dL)	0.88±0.15	0.88±0.16	1.73±0.33	5.09±1.91	**0.0013**
AST (IU/L)	21.4±3.03	55.50±9.01	51.63±6.81	60.43±11.52	**0.0111**
ALT (IU/L)	20.6±6.64	88.83±23.29	37.00±6.50	31.43±6.90	**0.0061**
Albumin (g/dL)	4.26±0.19	4.02±0.25	3.58±0.18	2.83±0.25	**0.0046**
Creatinine (mg/dL)	0.64±0.07	1.06±0.44	0.64±0.04	0.68±0.10	0.9903
INR	0.99±0.03	1.02±0.05	1.18±0.08	1.81±0.23	**0.0015**
MELD score	6.60±0.40	8.67±2.27	10.00±0.89	17.29±2.66	**0.0035**
p21 (IHC score)	3.70±0.43	27.59±3.94	55.79±7.31	102.4±7.24	**< 0.0001**
p53 (% positivity)	34.73±1.98	37.27±1.29	58.80±1.01	69.53±1.56	**< 0.0001**
LaminB1 (% intact nuclear membrane)	86.50±0.92	86.70±0.99	42.14±1.55	6.81±0.46	**< 0.0001**
γH2AX (IHC score)	53.13±2.72	80.00±6.44	133.5±3.16	239.6±4.87	**< 0.0001**
ClpP (intensity score)	1.00±0.0	0.33±0.21	2.94±0.63	1.71±0.29	**0.0001**
HSP60 (intensity score)	2.20±0.37	1.83±0.17	2.75±0.25	2.00±0.22	**0.0390**
HSP10 (intensity score)	2.00±0.32	1.67±0.21	2.75±0.16	1.29±0.18	**0.0024**

p values in bold indicate significant changes

Table 2. List of antibodies and various fluorescent dyes used in the study.

Antibodies	Catalogue no.	Lot no.	Dilutions		
			IHC /ICC	Immuno-fluorescence	Western blotting
p21	AM434-5M (BioGenex)	AM2391115	Ready to use	-	1:500
p53	AM239-5M (BioGenex)	AM2391115	Ready to use	-	-
Ki67	AM297-5M (BioGenex)	Clone MIB-1	Ready to use	-	-
$H_3K_9me_3$	ab8898 (Abcam)	GR186864-1	1:400	1:200	1:1000
γH2AX	ab26350 (Abcam)	GR90011-1	1:500	1:200	1:1000
GAPDH	G9545 (Sigma)	060M4775	-	-	1:5000
LaminB	sc-6216 (Santa Cruz Biotechnology)	F1812	1:100	1:50	1:500
CLPP	GTX104656 (GeneTex)	39708	1:200	-	1:500
HSP10	PAB501Hu01 (Cloud-Clone Corp)	A20170621181	1:20	-	1:250
HSP60	PAA822Hu01 (Cloud-Clone Corp)	A20170621167	1:20	-	1:250
Alexa Fluor 488 or 594 conjugated secondary (anti-mouse/rabbit/goat)	anti-M-488 A11029 anti-M-594 A11032 anti-R-488 A11034 anti-R-594 A11037	1503602 1420905 1423009 1420978	-	1:2000	-
Anti-Goat IgG-HRP	A5420 (Sigma)	whole molecule	-	-	1:3000
Anti-Rabbit IgG-HRP	170-6515 (BioRad)	whole molecule	-	-	1:5000
Anti-Mouse IgG-HRP	170-6516 (BioRad)	whole molecule	-	-	1:5000

Fluorescent dyes	Catalogue no.
Propidium iodide	349523 (BD Biosciences)
DAPI mounting media	H1200 (Vector Laboratories)
MitoTracker Red CMXRos	M7512 (Invitrogen)
MitoSOX	M36008 (Invitrogen)
Tetramethylrhodamine ethyl ester perchlorate (TMRE)	87917 (Sigma)

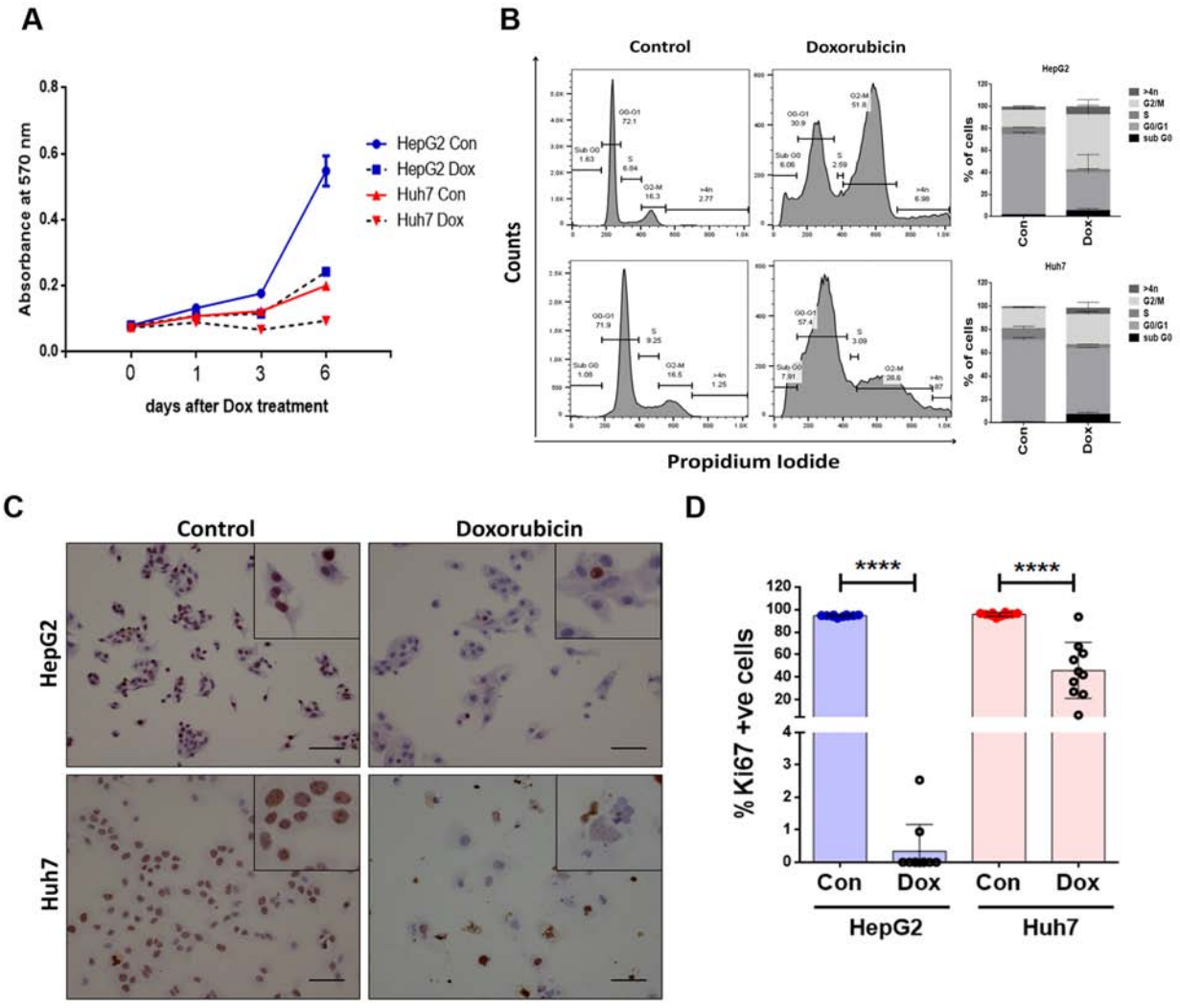

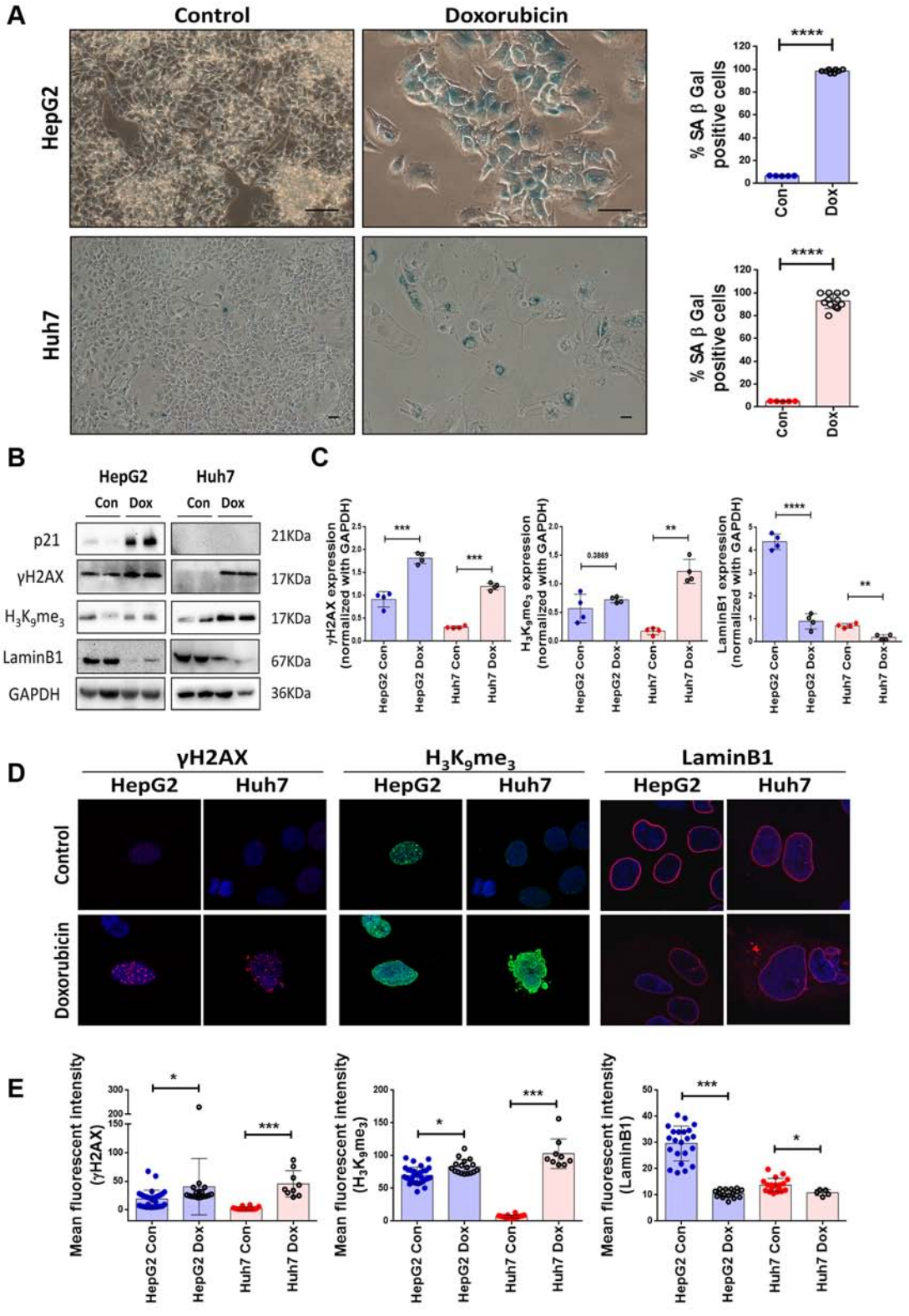
A
Control
Doxorubicin
HepG2
Huh7
% SA β Gal positive cells
Con
Dox
****
B
HepG2
Huh7
Con Dox Con Dox
p21
γH2AX
H3K9me3
LaminB1
GAPDH
21KDa
17KDa
17KDa
67KDa
36KDa
C
γH2AX expression (normalized with GAPDH)
H3K9me3 expression (normalized with GAPDH)
LaminB1 expression (normalized with GAPDH)
HepG2 Con
HepG2 Dox
Huh7 Con
Huh7 Dox
0.3869
D
γH2AX
H3K9me3
LaminB1
HepG2
Huh7
Control
Doxorubicin
E
Mean fluorescent intensity (γH2AX)
Mean fluorescent intensity (H3K9me3)
Mean fluorescent intensity (LaminB1)

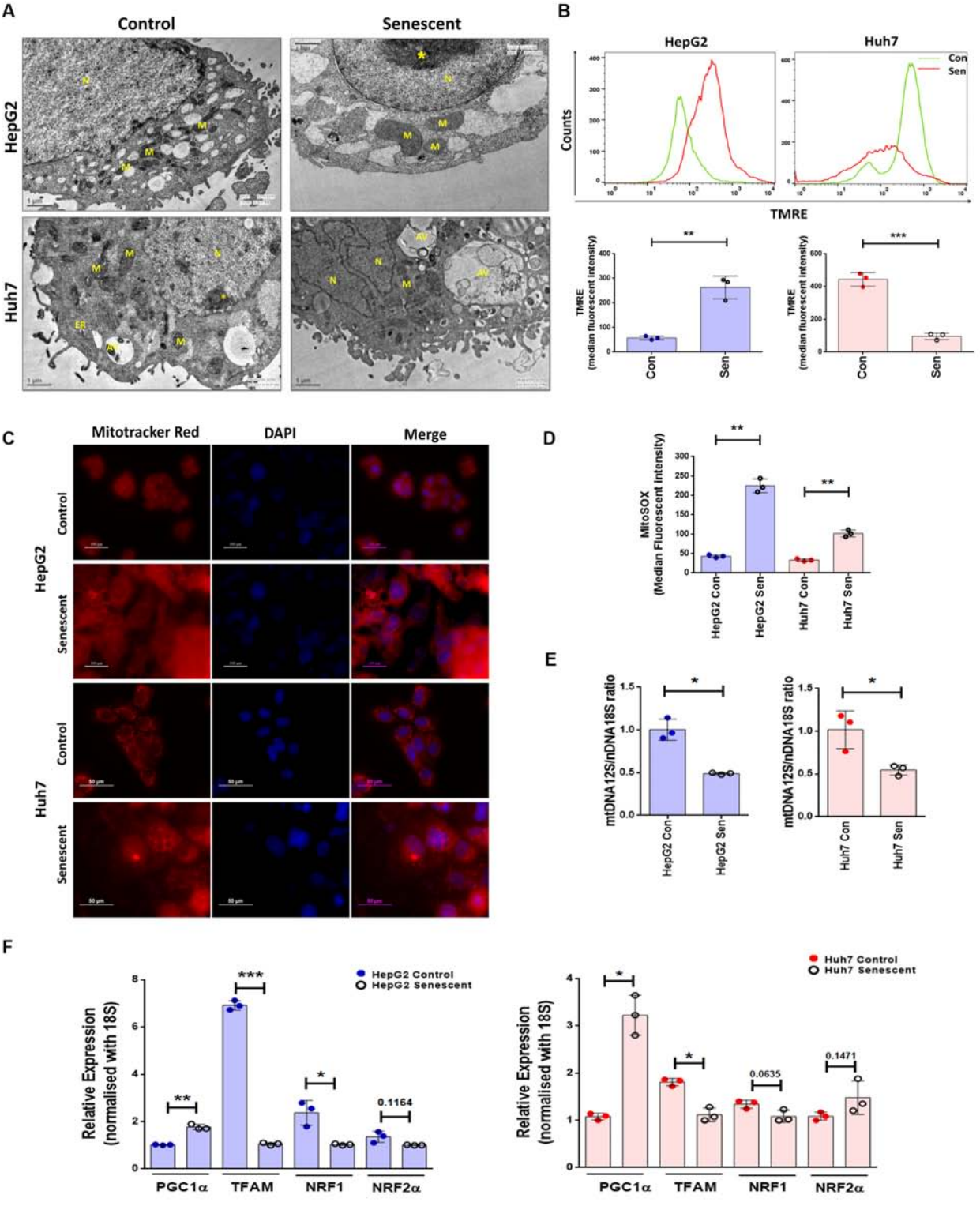
A
Control
Senescent
HepG2
Huh7
N
M
ER
AV
B
HepG2
Huh7
Con
Sen
Counts
TMRE
TMRE (median fluorescent intensity)
**
***
C
Mitotracker Red
DAPI
Merge
HepG2
Huh7
Control
Senescent
D
MitoSOX (Median Fluorescent Intensity)
HepG2 Con
HepG2 Sen
Huh7 Con
Huh7 Sen
E
mtDNA12S/nDNA18S ratio
F
HepG2 Control
HepG2 Senescent
Huh7 Control
Huh7 Senescent
Relative Expression (normalised with 18S)
PGC1α
TFAM
NRF1
NRF2α
0.1164
0.0635
0.1471

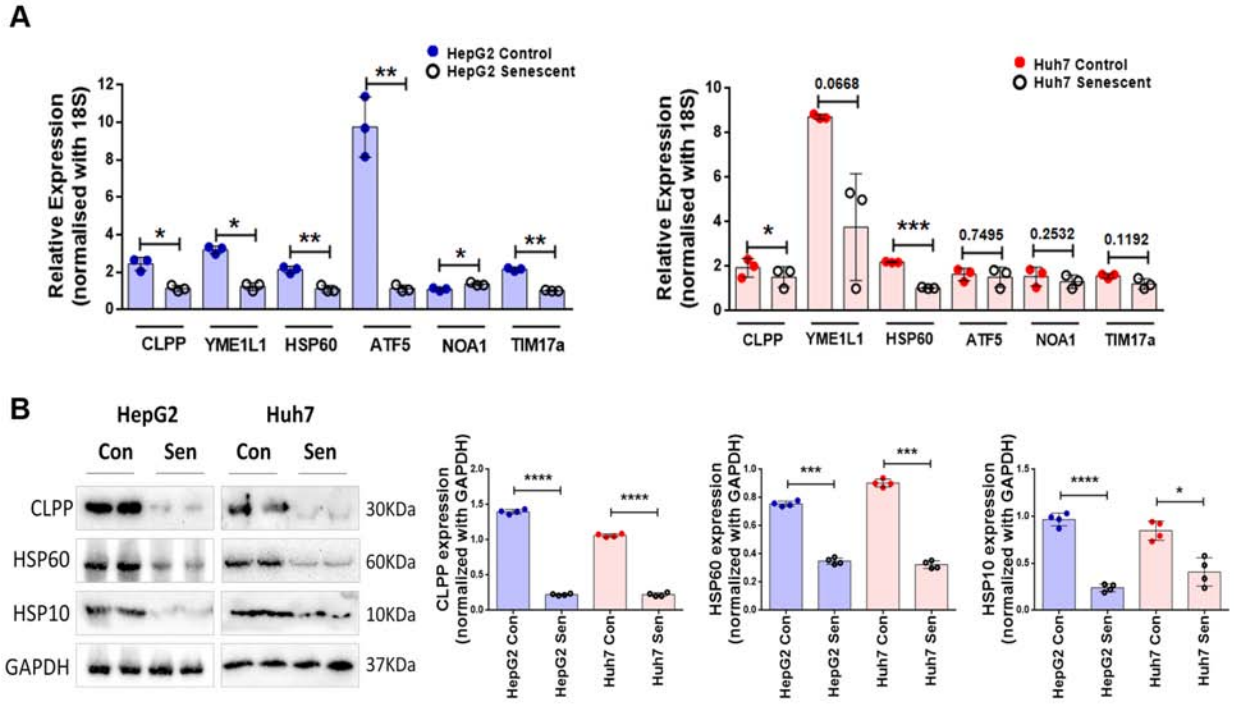

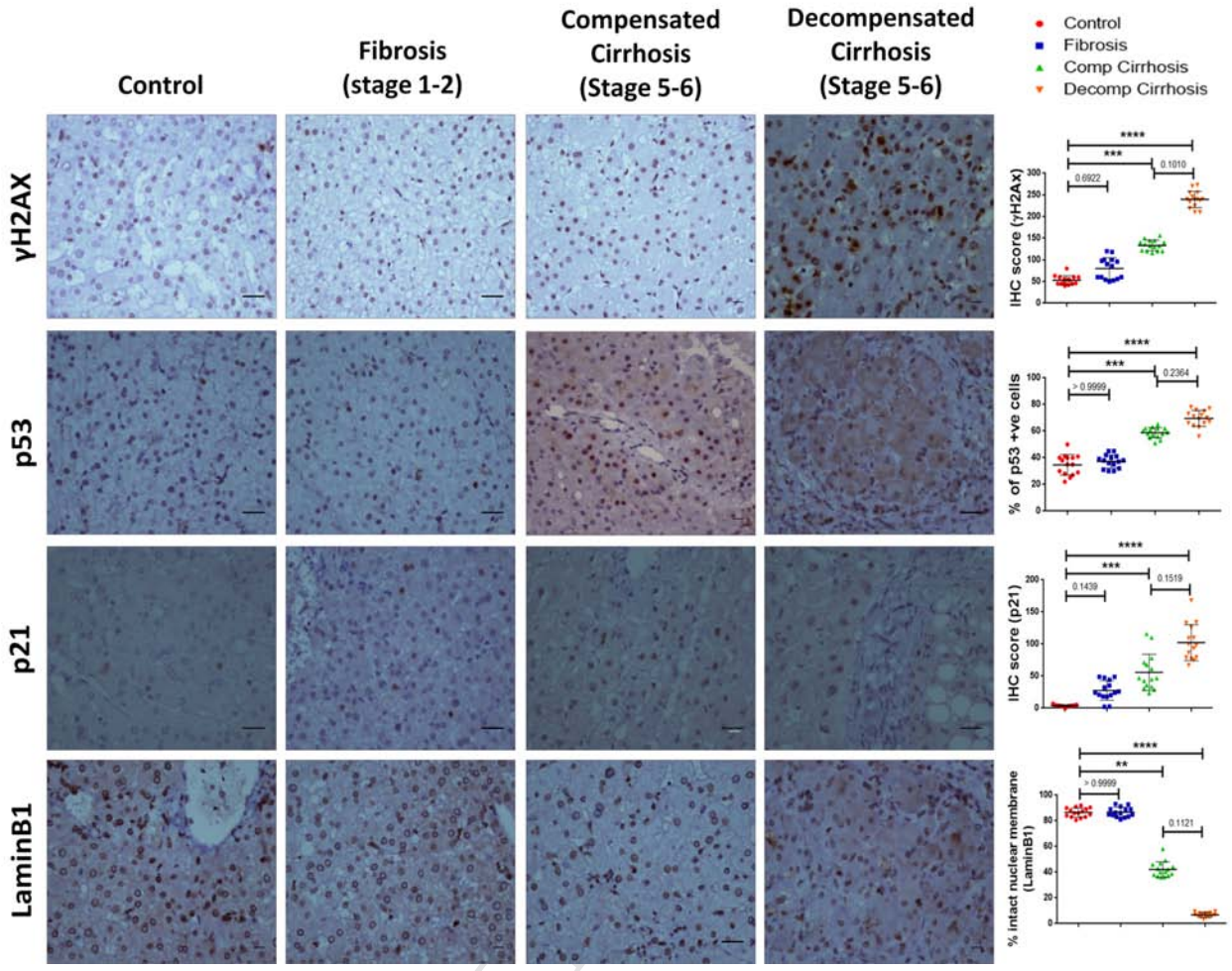
Control
Fibrosis (stage 1-2)
Compensated Cirrhosis (Stage 5-6)
Decompensated Cirrhosis (Stage 5-6)
Control
Fibrosis
Comp Cirrhosis
Decomp Cirrhosis
γH2AX
p53
p21
LaminB1
IHC score (γH2Ax)
% of p53 +ve cells
IHC score (p21)
% intact nuclear membrane (LaminB1)
****
***
**
0.6922
0.1010
> 0.9999
0.2364
0.1439
0.1519
0.1121

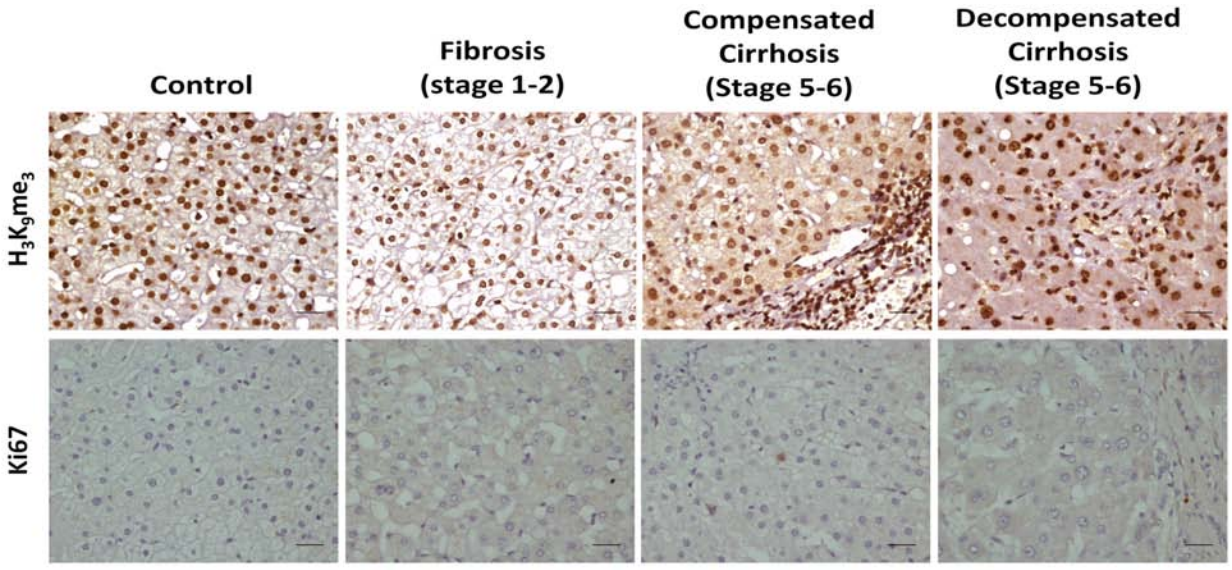

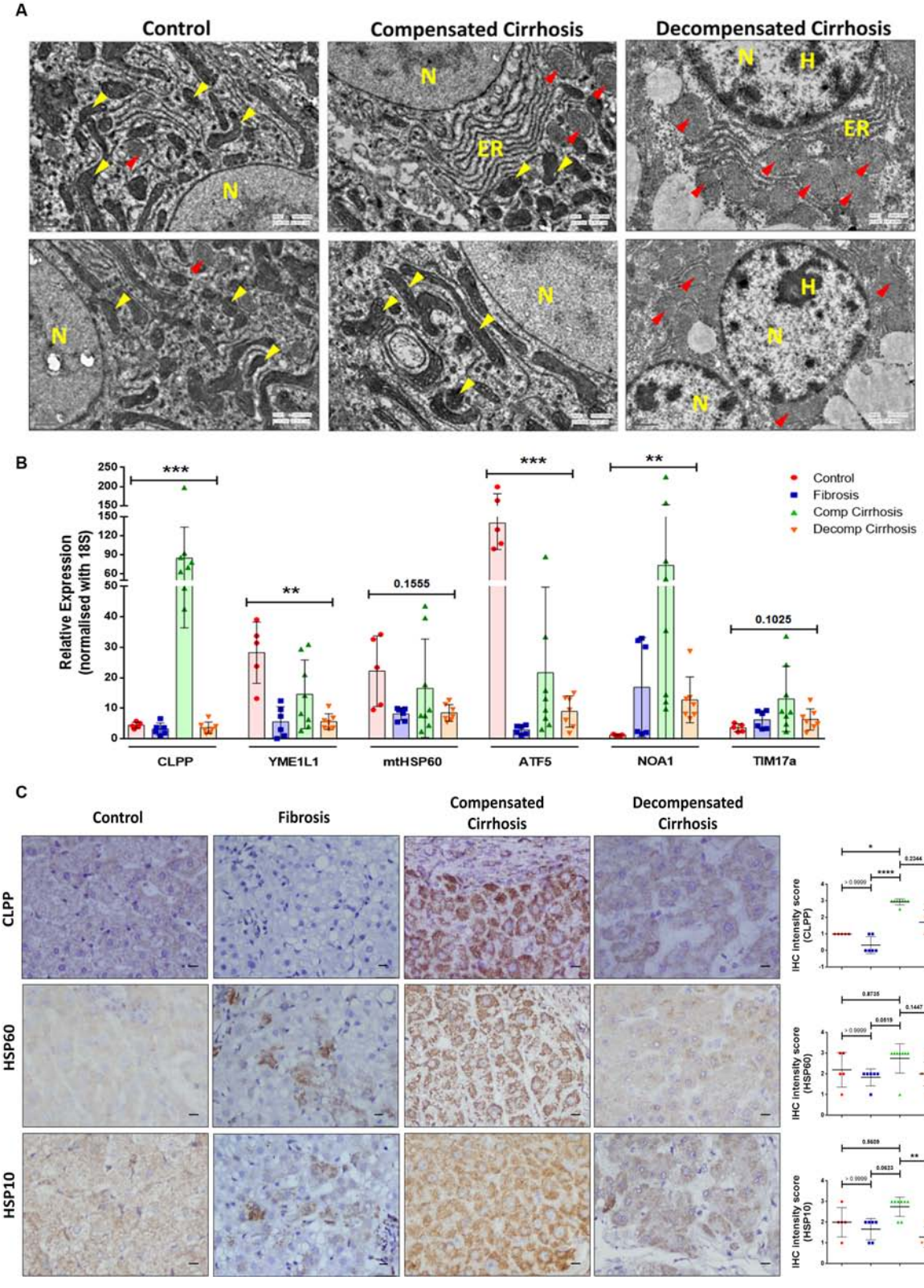
A
Control
Compensated Cirrhosis
Decompensated Cirrhosis
N
ER
H
B
Relative Expression (normalised with 18S)
Control
Fibrosis
Comp Cirrhosis
Decomp Cirrhosis
***
**
0.1555
0.1025
CLPP
YME1L1
mtHSP60
ATF5
NOA1
TIM17a
C
Control
Fibrosis
Compensated Cirrhosis
Decompensated Cirrhosis
CLPP
HSP60
HSP10
IHC intensity score (CLPP)
IHC intensity score (HSP60)
IHC intensity score (HSP10)

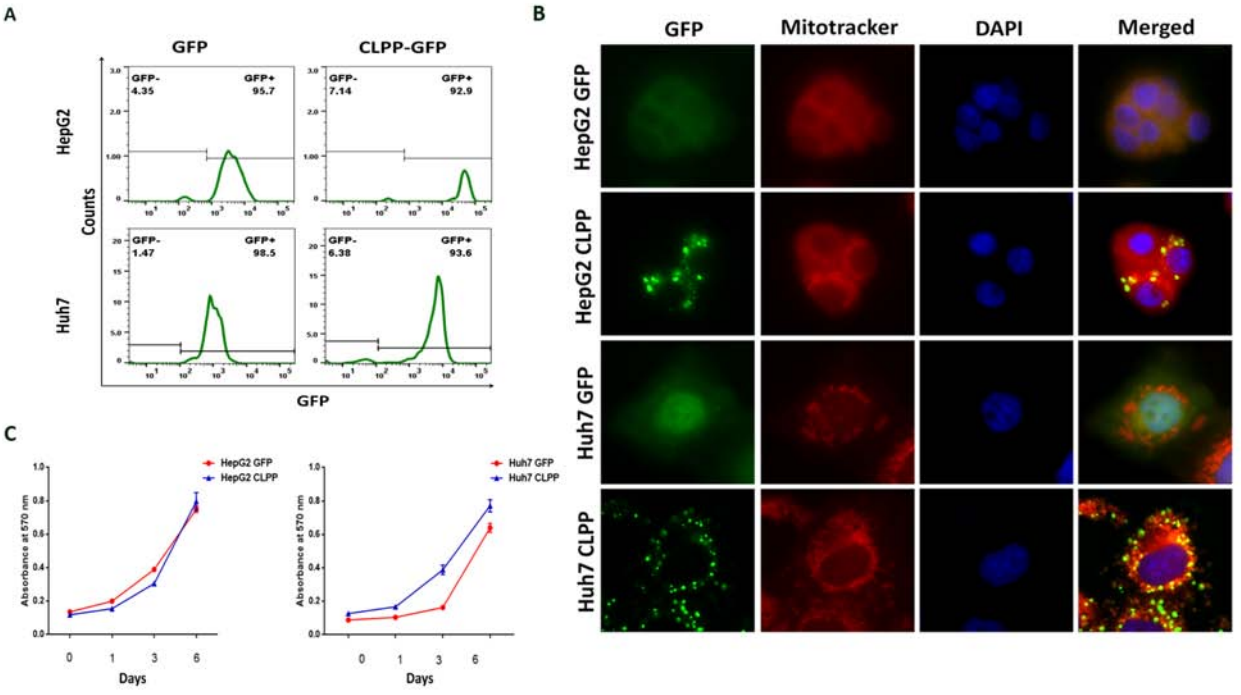

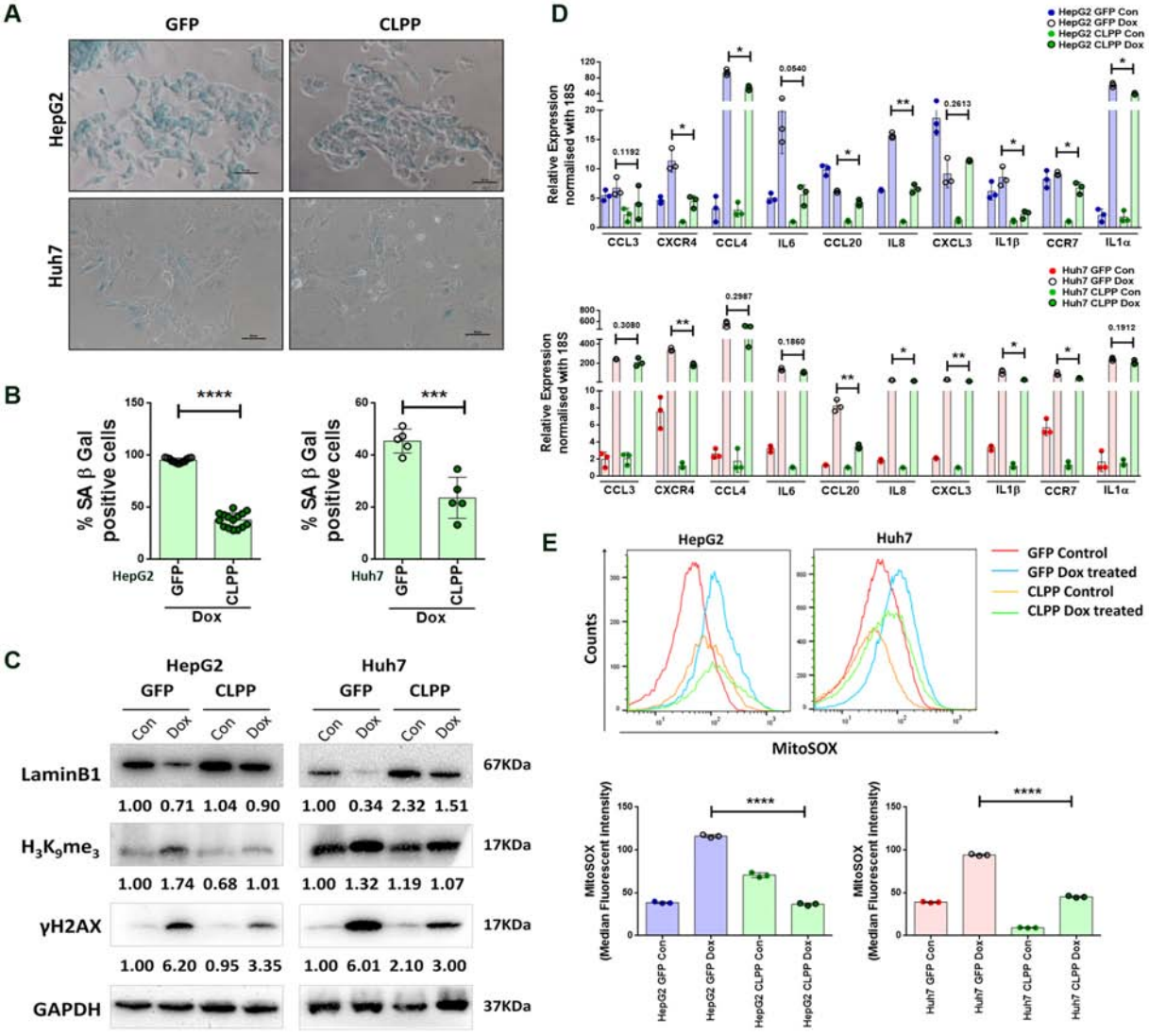

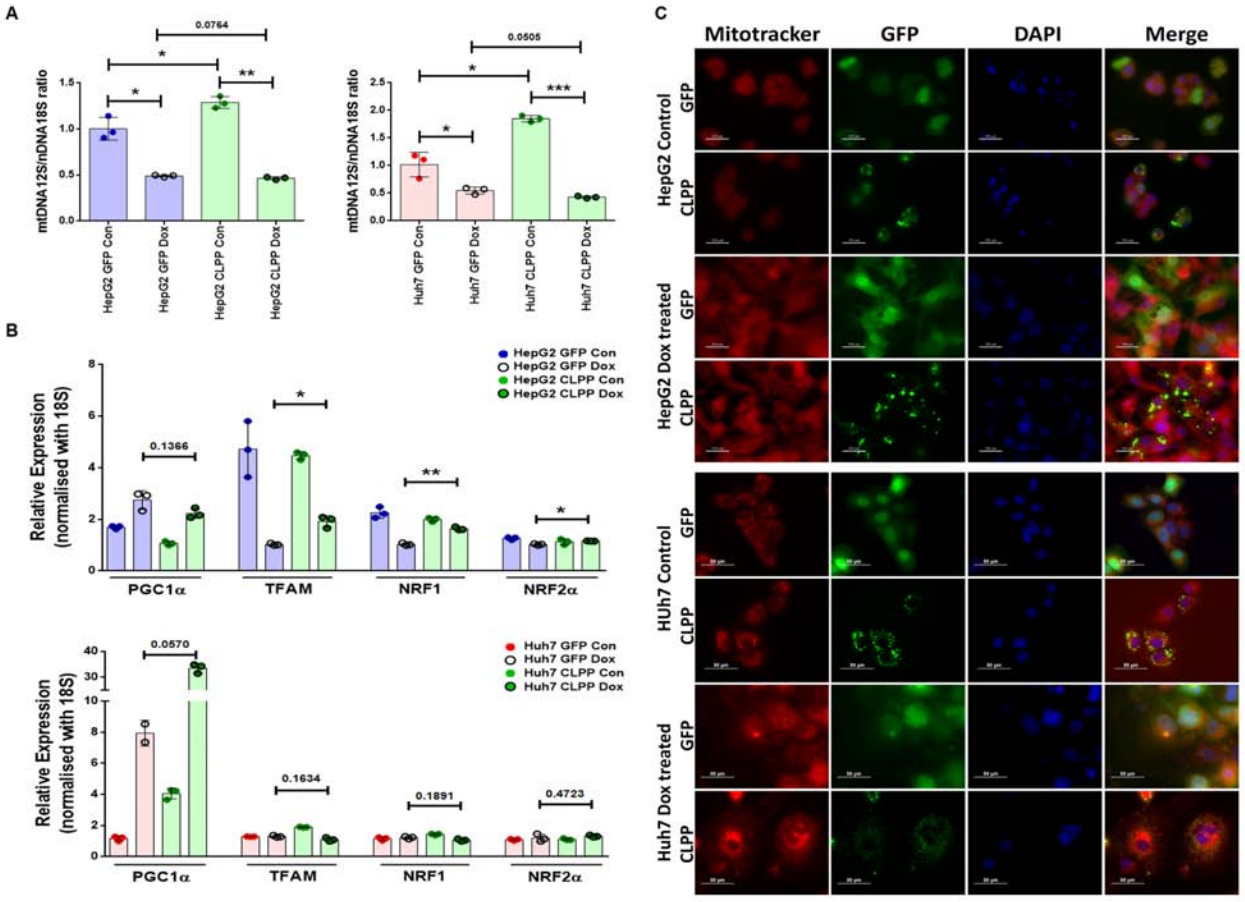
A
mtDNA12S/nDNA18S ratio
0.0764
*
*
**
HepG2 GFP Con
HepG2 GFP Dox
HepG2 CLPP Con
HepG2 CLPP Dox
0.0505
*
*
***
Huh7 GFP Con
Huh7 GFP Dox
Huh7 CLPP Con
Huh7 CLPP Dox
B
Relative Expression (normalised with 18S)
HepG2 GFP Con
HepG2 GFP Dox
HepG2 CLPP Con
HepG2 CLPP Dox
0.1366
*
**
*
PGC1α
TFAM
NRF1
NRF2α
Huh7 GFP Con
Huh7 GFP Dox
Huh7 CLPP Con
Huh7 CLPP Dox
0.0570
0.1634
0.1891
0.4723
C
Mitotracker
GFP
DAPI
Merge
HepG2 Control
HepG2 Dox treated
HUh7 Control
Huh7 Dox treated
GFP
CLPP

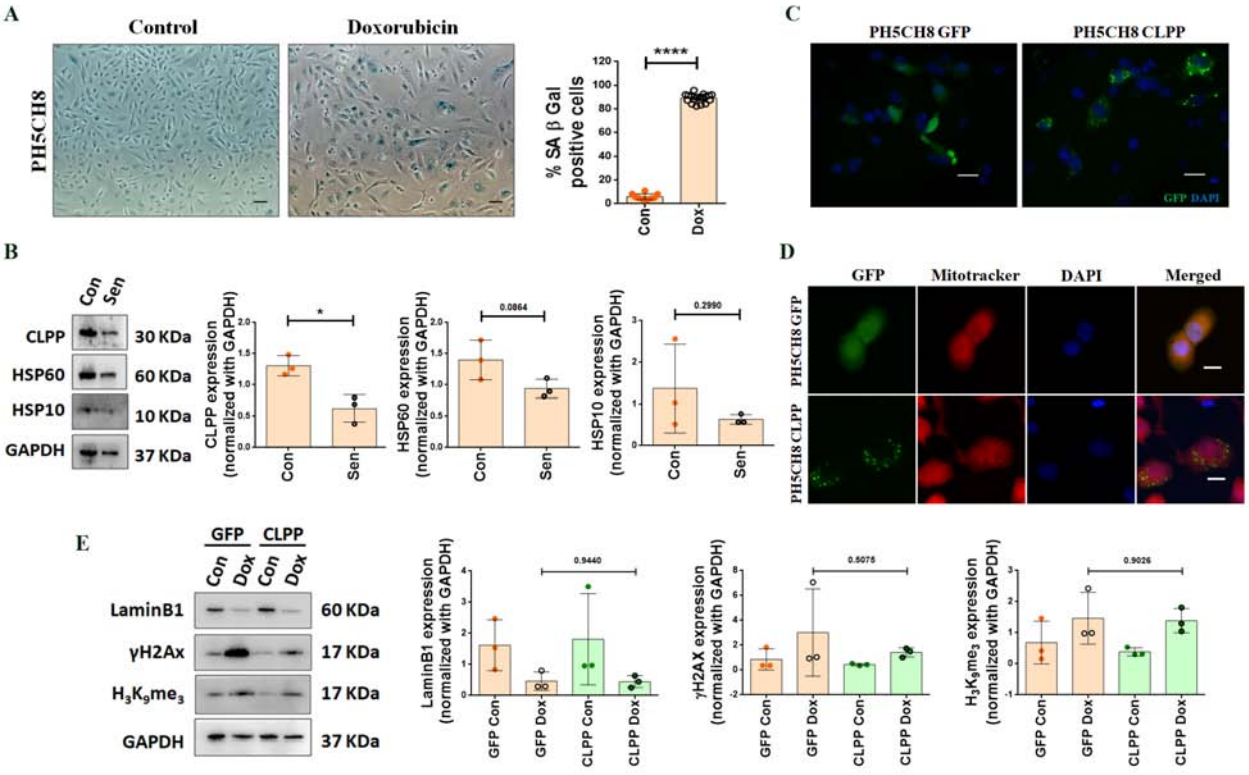

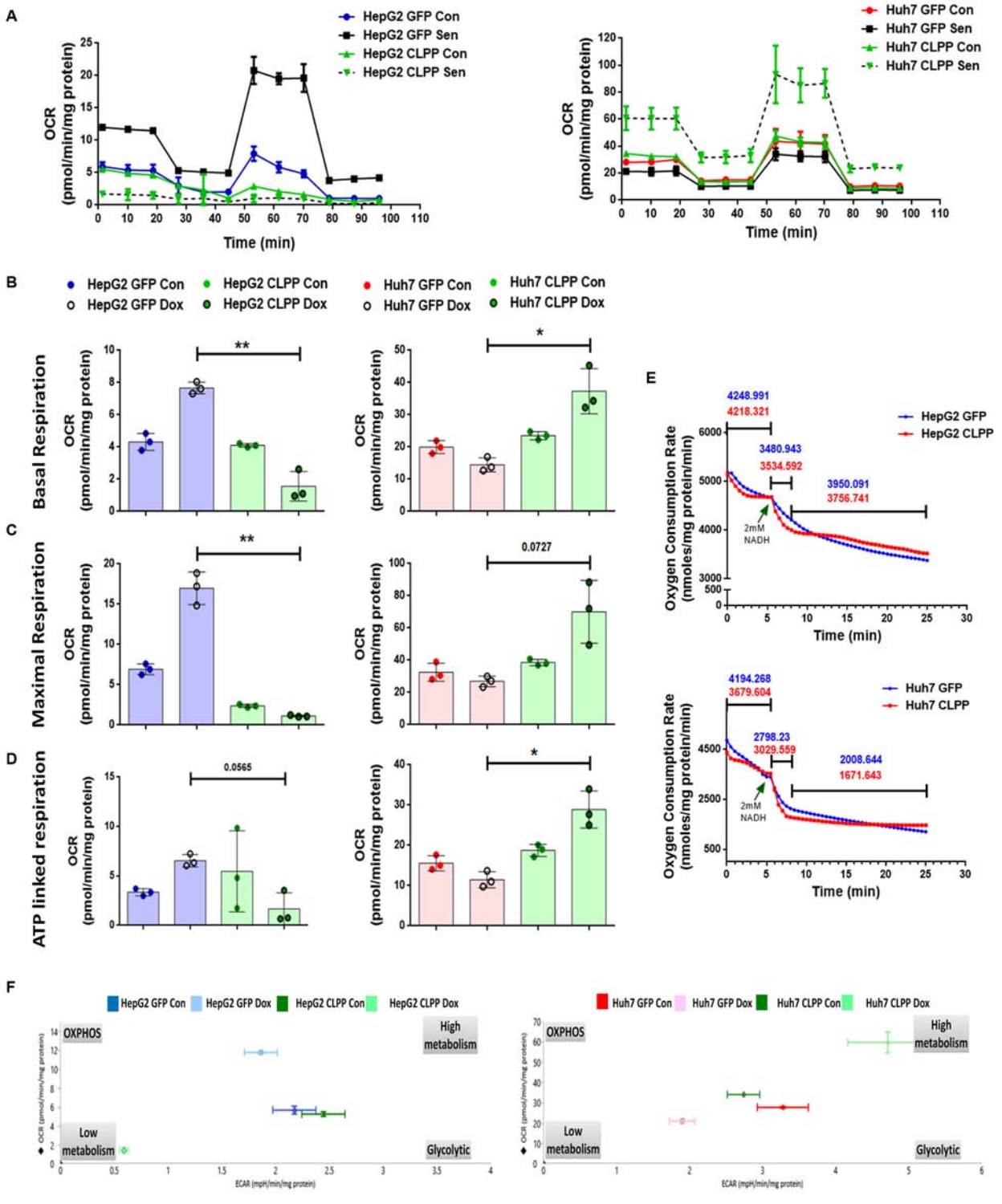
A
HepG2 GFP Con
HepG2 GFP Sen
HepG2 CLPP Con
HepG2 CLPP Sen
OCR (pmol/min/mg protein)
Time (min)
Huh7 GFP Con
Huh7 GFP Sen
Huh7 CLPP Con
Huh7 CLPP Sen
B
HepG2 GFP Con
HepG2 GFP Dox
HepG2 CLPP Con
HepG2 CLPP Dox
Huh7 GFP Con
Huh7 GFP Dox
Huh7 CLPP Con
Huh7 CLPP Dox
Basal Respiration
C
Maximal Respiration
D
ATP linked respiration
**
*
0.0565
0.0727
E
4248.991
4218.321
3480.943
3534.592
3950.091
3756.741
2mM NADH
Oxygen Consumption Rate (nmoles/mg protein/min)
HepG2 GFP
HepG2 CLPP
4194.268
3679.604
2798.23
3029.559
2008.644
1671.643
Huh7 GFP
Huh7 CLPP
F
OXPHOS
High metabolism
Low metabolism
Glycolytic
ECAR (mpH/min/mg protein)